Department of Precision and Microsystems Engineering

Design and stability analysis of an optic flow controller for the hover of the atalanta flapping wing micro aerial vehicle

Frank D. van Raalte

Report no	: 2024.050
Coach	: Dr.ir. J.F.L. (Hans) Goosen
Professor	: Dr.ir. J.F.L. (Hans) Goosen
Specialisation	: ME & MSD
Type of report	: Master Thesis
Date	: 9 July 2024

TUDelft Delft University of Technology

Challenge the future

Abstract

Over the past decades the increased use of Micro Aerial Vehicles (MAV's) in a large range of fields and applications has lead to a call for more energy efficient MAV's. Here Flapping Wing Micro Aerial Vehicles (FWMAV's) offer the possible solution since it was shown that animals such as colibris and insects have very energy efficient flight mechanics. The drawback of these currently developed FWMAV's is that they have limited lift generation. This limits the energy that can be carried in the form of batteries. This posses limits on the amount of energy that can be spent on both control and sensing. One solution is to use insect inspired optic flow sensors and a simplistic control method to directly control the velocity, instead of using the standard acceleration and GPS measurements. The insect inspired optic flow sensors allow for the measuring of velocity over distance relation. This method allows for a controller to take advantage of the sensor behaviour in order to increase responsiveness close to walls or at high velocities without need for complex control methods. With this goal in mind, two different sensor control variations were developed and tested in a simulation environment. Here the effect of different parameters and conditions were studied and analysed in order to evaluate the effectiveness and potential of these controllers and the general control approach. Analysis show that the behaviour of both controller respond slightly differently on the change in the initial position for a given initial velocity. The implementation of a more realistic sensor did result in different behaviours for certain initial conditions.

Contents

List of Figures

Nomenclature

Abbreviations

Abbreviation	Definition
FWMAV	Flapping wing micro aerial vehicle

Symbols

Symbol	Definition	Unit
A	Amplitude of the curve fit	[]
c	curve fit offset constant	[]
C	general controll signal	[]
C^{I^+}	Curl optic flow of the positive I facing sensor	[1/s]
C_{w_1}	Control signal of wing 1	[]
d	decay distance	[m]
D^{I^+}	Divergence optic flow in the I direction	[1/s]
f	focal distance	[m]
$gain_{rot}$	Rotational controller gain	[s/m]
$gain_{trans}$	Translational controller gain	[s/m]
$h(x)$	position dependent realistic sensor decay	[]
$OF_j^{I^+}$	Direct optic flow in the j direction of the positive I sensor	[1/s]
r^{I^+}	distance of the positive I facing sensor to the wall	[m]
$\vec{r}_{p1}^{I^+}$	principle direction 1 of the positive I facing sensor	[]
$\vec{s}_{p1}^{I^+}$	principle direction 1 of the observed wall of the positive I facing sensor	[]
t	time	[s]
$\vec{v}$	velocity of the atalanta	[m/s]
$\vec{v}^i$	The velocity of the divergence sensor in I direction	[m/s]
$\vec{v}_j^{I^+}$	The velocity in j direction of the direct sensor in I direction	[m/s]
$\vec{v}_i$	controller velocity in i direction	[m/s]
$v_{p1}^{I^+}$	The magnitude of the velocity observed by positive sensor I in principle direction 1	[m/s]
ψ	yaw	[rad]
θ	pitch	[rad]
ϕ	roll	[rad]
$\omega_j^{I^+}$	rotational velocity around the j axis observed by the I facing direct sensor	[rad/s]
ω^{I^+}	rotational velocity around the positive I axis observed by the positive I facing sensor	[rad/s]
λ	curve fit decay factor	[1/s]
ω_i	controller rotational velocity around the i direction	[1/s]

1

Introduction

This thesis aims to develop and test a control algorithm for the Atalanta flapping wing micro aerial vehicle using. First the background and basic principles will be discussed in order to show the relevance of this research and allow for in depth discussion of the results.

1.1. Introduction to (FW)MAV's

Over the past few decades, the development of new technologies for unmanned aerial vehicles (UAV) has led to the increasing request for the down scaling of the UAVs. These smaller UAVs called micro aerial vehicles (MAV) show a lot of promise where their larger counterparts have limited operating capabilities. MAVs show their promise mostly in the area concerning indoor operation where the small size and high manoeuvrability make it much easier to navigate corridors and avoid obstacles, common in indoor environments. Secondly MAVs show promise as (autonomous) sensor platforms, in this application they are fitted with sensor such that they can take localized measurements of the environment. Such sensor platforms can be used both independently and in a swarm configuration [1]. Lastly MAVs show promise in the field of surveillance and reconnaissance, due to their small size they can easily go undetected.

In the area of MAVs, the distinction can be made between MAV's that use some form of rotor to generate the propulsion needed for flight, such as airplanes or quadcopters, and MAVs that make use of flapping wings called flapping wing micro aerial vehicles (FWMAVs). These FWMAVs often find their inspiration in the world of biology. Insects such as flies or small birds such as the hummingbird are some of these inspirtations. Over the last two decades many projects have worked on developing FWMAVs with different approaches and goals in mind.

1.2. The advantage of the FWMAV

FWMAVs show multiple advantages over other MAVs. The biggest advantage compared to other MAVs stems from a FWMAVs agility and manoeuvrability without compromising its ability to hover. Rotor MAVs with fixed wings resembling planes are often not even capable of hovering and those such as quadcopters have relatively low manoeuvrability because their rotors can only generate upwards lift, requiring more advanced control to move forward or sideways. For FWMAVs lift is not generated purely upwards allowing for more manoeuvrability. FWMAVs have, compared to rotor MAVs a relatively low power consumption [the novel aerodynamics of insect flight: applications to micro-air vehicles][7] allowing for more efficient flight, larger payloads or more sensors.

1.3. The Atalanta

In 2010 C. Bolsman proposed the development of one such FWMAV that makes use of a resonant compliant mechanism to actuate the wings. The goal of this project, called the Atalanta project, is to create an autonomous FWMAV capable of both hover and slow flight. It should eventually be able to carry a payload, manage power storage and communicate with a base station. The aim is for the atalanta to have a wingspan of 100 mm and a mass of 4 gram[2]. Based on the initial research done by

Bolsman, three major aspects related to the Atalanta can identified. Namely the area involved with the understanding of the (aero)dynamics of the atalanta and the development of an appropriate model, the aspect concerned with overal design of the atalanta and its wings and lastly the development of a control setup for the control of both hover and flight.

Research into the (aero)dynamics of the Atalanta has led to the refinement of the dynamical model that can be used to describe the Atalanta, an example of this is the development of a quasi-steady state model for the wings by Wang[Modeling, design and optimization of flapping wings for efficient hovering flight.] in order to model the thrust generated by the flapping wings of the MAV, which was further refined by Kottiswaran [19] in an attempt to add the effects of translational and rotational flight to the modelled thrust.

Related to the design of the Atalanta, Menkhorst has developed an improved design of the Atalanta by bringing theory into practice. [22]. The developed prototype shows promising lift generation but is limited by the amount of energy it is able to store. This limited energy storage results in a flight time of only 1 or 2 seconds before running out.

The research has also investigated the control of the Atalanta whereby the focus has been on insect inspired control using optic flow sensors. This insect inspired sensor method has the advantage of relatively simplistic control and therefore requiring a lot less power than in standard control methods. Van Vrede has shown that it is possible to effectively use optic flow in a simplistic control loop to control a quadcopter[31].With the limited power availability this control method might be the way forward when it comes to low energy, robust control.
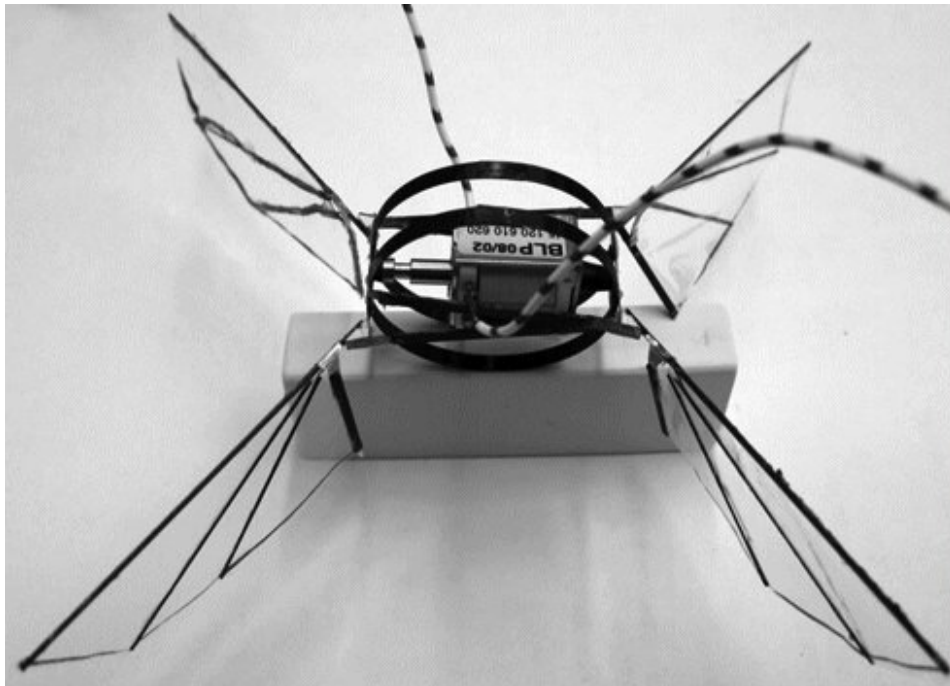
Figure 1.1: The Atalanta FWMAV [2]

1.4. Other FWMAVs

With the rising interest in FWMAVs have come a large number of projects taking inspiration from different insects or animals in an attempt to obtain flapping wing flight. Projects have shown different areas of focus in which they have aimed to improve or develop a FWMAV. Some of these projects will be breifly discussed for their uniqueness or relevance to the atalanta project. A more complete list of different FWMAV projects can be found in Appendix A.

One of the first FWMAVs to attain flight was the Harvard microfly[32], which at just 60 mg used a piezo actuator to obtain uncontrolled flight putting the focus on the small size, with no focus on control. This project showed what might be possible and the direction in which the research was headed. The delfly project [6][16] started out as a student project to participate in a MAV competition, but has grown

to be one of the most successful projects when it comes to autonomous MAV flight. The project first aimed at creating a unique MAV design, but later focused on down scaling and the development of an autonomous flying MAV. The delfly nimble obtained completely autonomous flight with a wingspan of 33 cm and a mass of 28.2 gram. Capable of flight similar to that of a fruit fly, it can avoid obstacles and make almost 90 degree turns. These results from the delfly are similar to the goals set for the Atalanta, however with a larger MAV and heavier MAV. The eMotionButterfly[8] developed by Festo aimed to get as close to lifelike flight as possible by attempting to use the smallest installation space possible. This new design and flight behaviour brings Festo one step closer to intelligent networked flight. This design also shows the unique qualities of insect mimicking flight in its capability to glide, only flapping periodically and therefor using less energy. Lastly the robobee x-wing [14] has shown a possible route to long term wireless flight by using ultra lightweight solar panels as a power source while using piezoelectric actuators to drive the wings. The robobee x-wing generated more lift than needed for manoeuvrability and hover, suggesting the possible addition of on board control components or batteries. The current design however, uses more power than can be obtained from the solar panels with sunlight making practical applications currently nonviable, but it has opened the door for further development of solar powered MAVs and the possibility of long term flight without big batteries.

(a) The harvard microfly developed by harvard university.[32]

(b) The robobee x-wing developed by harvard microbotics lab.[14]

(c) The delfly nimble developed by Delft university of technology.[16]

(d) The delfly micro by Delft university of technology.[6]

(e) The eMotionButterfly by Festo AG & Co. KG.[8]
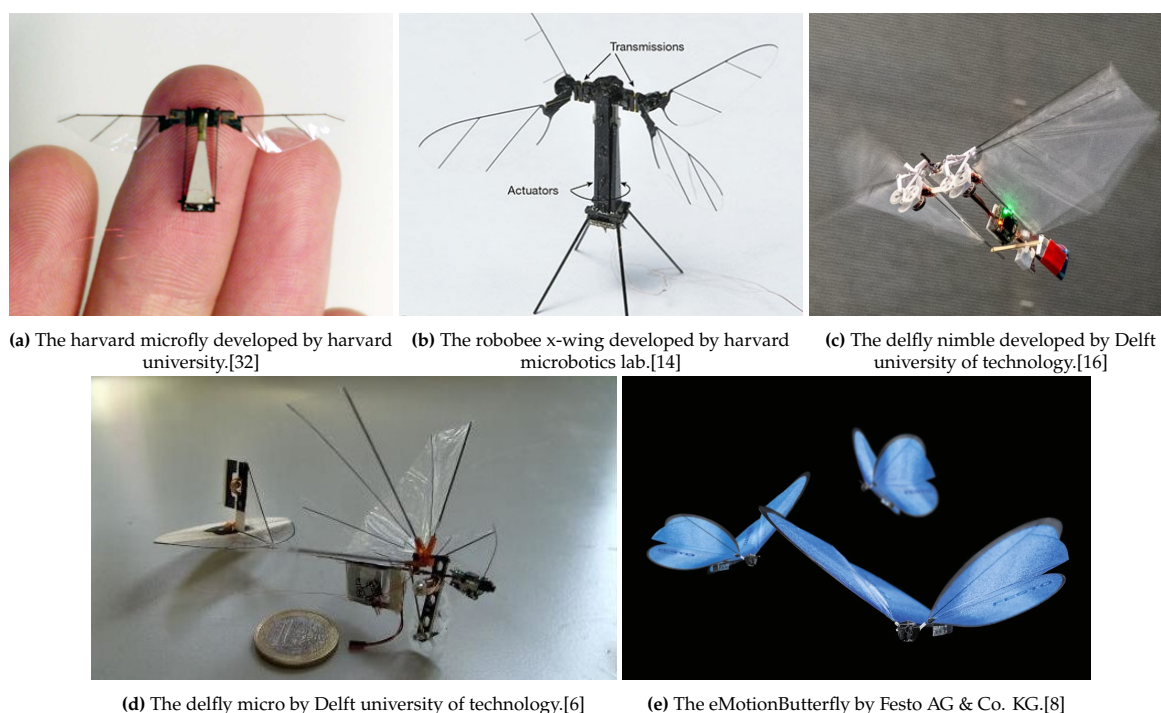
Figure 1.2: Different FWMAV projects of interest or significance

1.5. Optic flow

There are different methods to calculate optic flow, the most basic method to calculate optic flow is to assume the brightness of light is constant across the image and the optic flow within the image is given by a smooth vector field. Using these assumptions and estimating the partial derivatives and Laplacians result in an error equation. By minimizing this error an estimate of the optic flow within an image can be obtained as demonstrated by Horn and Schunck [13]. A more refined approach assumes that the brightness is not constant across the image but varies smoothly in an attempt to decrease errors in the optic flow due to lighting conditions.[18] Both methods result in the optic flow vector field across the image. These vector fields can contain a lot of information on the local movements of objects within the frame, as well as the relative motion of the environment to the sensor. Figure 1.3 shows the relationship between the motion of an insect and the perceived optic flow field. In applications such as flight control the motion of the environment is more important for obtaining basic attitude and altitude control compared to that of moving objects. In order to obtain an indication of these large movements, the
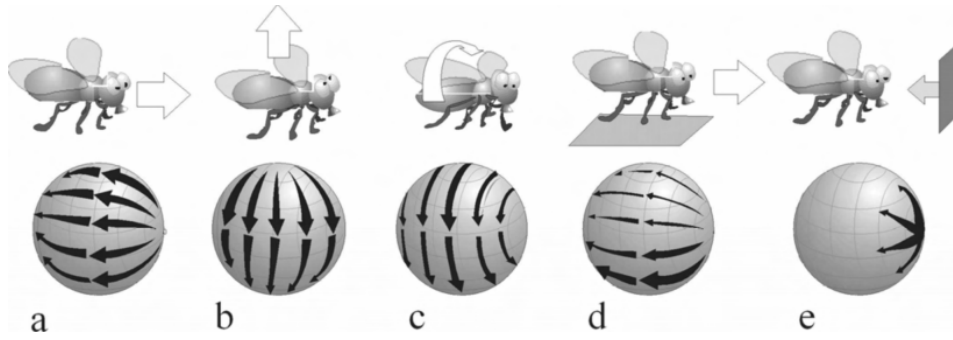
Figure 1.3: The relation between motion and optical flow fields[9]. a) forward motion, b) upward motion, c) leftward roll, d) flow speed difference due to surface proximity, e) outward flow caused by approaching surface.

vector fields can be converted into two values corresponding to the optic flow along the principal axis of the sensor. These values have a relation to the motion of the observer relative to the image as described by Equation 2.4. Here v is the velocity parallel to the principal axis, r is the distance from the sensor to the wall perpendicular to the sensor surface, alpha the angle between the wall and the velocity vector and omega the rotational velocity in the plane spanned by the velocity and distance vector. The x, y and z indicate the axis along or around which the distance, velocity and angular velocity operate and X, Y and Z indicate the axis on which the sensor is located with a + or - to indicate the negative or positive direction along which the sensor is oriented.

$$OF_z^{X^+} = \frac{v_z}{r^{X^+}} * \sin \alpha^{X^+} + \omega_y \tag{1.1}$$

An alternative is to compute the divergence of the optic flow fields which has a linear relation with velocity and an inverse relation with distance as shown in Equation 1.2. The method suggested by Ho et al.[11]][12] makes use of a full image camera and corner and edge tracking within this image to determine the divergence within the image but is also applicable on an optic flow vector field to determine the divergence within this field. Alternatively to the computer intensive method described by Ho et al. the divergence can also be calculated using the vector field obtained from the optic flow sensor.

$$D^{X^+} = \frac{v_x}{r^{X^+}} \tag{1.2}$$

These methods can provide information on the relative movement of the environment with respect to the MAV. Using this information on relative movement might prove beneficial in navigating a three-dimensional environment with a relatively simple control loop. The advantage of using optic flow along the principle axis is that it can also provide insight into the rotational motion of the sensor and FWMAV due to the presence of the angular velocity within Equation 1.1. Divergence optic flow does not provide this insight, but only provides information on the translational motion, rotational motion is unobservable using divergence. If insight into the rotational motion is desired, it might be of interest to look further into the possibility of using curl, the rotational complement to divergence.

When using optic flow it is important to take into account that optic flow is sensitive to light and general contrast conditions of the consecutive images. This means that single colour walls, which has a very low contrast, gives low optic flow values even for large motions, while high contrast will result in larger optic flow values for smaller motions. Light can also affect the optic flow output in one of two ways. First a moving light source might give the output of apparent motion due to the changing contrast region caused by the movement of the bright spot of the light. Secondly light levels can affect the contrast in the image by either over or under illuminating certain regions, causing the same motion to give different optic flow results under different lighting conditions. These external influences might affect the accuracy and effectivness of optic flow sensors in certain conditions.

1.6. Control
In order to make flight of FWMAVs possible the FWMAV needs to be controlled. Control can be done using different approaches, namely using full remote control by a remote pilot, partial control by a

remote pilot with partial sensor control, fully autonomous flight using sensors or uncontrolled flight in which the FWMAV takes no external inputs. In the case of the Atalanta the focus is on partial or fully autonomous control for which different approaches are discussed.

1.6.1. Standard control

Some of the FWMAVs, such as the delfly, have a form of control to make it possible to autonomously hover and sometimes even navigate spaces. Most of these control networks make use of closed loop feedback, often using a form of a PID controller. Sometimes using filters or other more complex control operations to allow the FWMAV to operate autonomously. These advanced control loops take a lot of computing power and energy, which is limited on a FWMAV, making it one of the limiting factors of FWMAV development.

One of the reasons such complex control is needed for FWMAVs is because the only input we can give to the system is acceleration, while often wanting to control position or velocity. This means that in order to control the position double integration is needed with respect to the sensor data and in order to hover at an arbitrary point at least one integration operation is needed. This numeric integration will over time introduce an error to the system and cause computer delays, reducing controblability and lowering the accuracy.

1.6.2. Optic flow control

An alternative to the commonly used advanced control loops is suggested by Goosen [9], namely, to use optic flow sensors with direct control for the autonomous operation of the FWMAVs. The possible advantage of optic flow as suggested by Goosen stems from the fact that it measures the ratio between velocity and distance to the object. Goosen suggests that in the case of hover simplistic linear feedback might suffice without any large deviations. De Croon [5] has shown that it is possible to obtain a state of stable hovering using purely optic flow when the gain is adequately adjusted to the operating space and the system is operating relatively far away from the walls. Serres and Ruffier [29] have also shown that optic flow can be used to avoid objects in the travelling path when computing.

The simple linear direct optic flow control method shows promise when the desired knowledge of the velocity and position is limited. If knowledge of position and velocity are desired, they need to be extracted from the optic flow data using more complex methods, for example using a prescribed acceleration pattern and the derivative of the optic flow. The simple linear control method also breaks down when the MAV comes close to one of the walls or under heavy external disturbances as shown by Van Vrede[31].

A slightly more advanced control loop might offer the solution to the limits of the basic control as mentioned above, while still using the data received from optic flow. A list of possible different methods is made in order to evaluate the possibilities of these different approaches and their strength and weaknesses, which can be used to select directions for further research.

- Using model prediction to keep an estimate of the system's position and velocity.
- Use a known acceleration profile to estimate the current distance to the walls and current velocity
- Using change in contrast to estimate distance to the walls.
- Use the property of self-induced oscillations to determine the distance to the walls[5].
- Using constant divergence to keep or change distance to the walls.

Model prediction is a method used in a lot of high precision positioning applications. This approach uses knowledge of the dynamic model to determine the needed input forces to obtain the desired output position. The advantage of this method is in the fact that you can control multiple outputs at the same time since you are aware of the interactions between the different variables. This method however is computing intensive and requires very accurate knowledge of both the state and the dynamic model of the system you are controlling, which is often not the case for FWMAV's.

An alternative is to use a known acceleration profile in order to the determine the distance to the different walls. This method attempts to estimate the current velocity and distance to the walls by using the derivative of the optic flow and a known acceleration profile. This method is relatively simple compared to the previously mentioned method, but still requires accurate knowledge of at least the

acceleration behaviour of the FWMAV and is highly dependent on the contrast and light levels within the field of view of the sensors.

Using the change in contrast might give us insight in the position estimation of the FWMAV allowing us to control this position using a simple control loop. This method is less computing intensive, but is highly dependent on light conditions and the surface texture of the walls.

De Croon [5] has shown that by tuning the gain on the simplistic control method a set distance to the walls or floor can be obtained. The gain of the control loop is lowered until the FWMAV starts showing oscillatory behaviour due to the onset of instability. Where each gain corresponds to a given distance. This method is more simplistic in providing insight into the distance to the walls compared to the acceleration pattern method since it needs no real knowledge of the actual dynamics of the system, however this method places the FWMAV on the border of instability where even small changes can cause the system to become unstable.

The last method attempts to control the FWMAV by setting the divergence of the optic flow field either to zero when hovering or a fixed value when attempting to move in a given direction. Due to the nonlinear relation between distance to the wall and divergence, as discussed in Section1.5, the FWMAV will inherently slow down when coming close to a wall. When divergence is set to zero for two opposite sensors, the FWMAV should obtain a hovering state. Since the only way to bring Equation 1.2 for both the positive and negative looking sensor is by bringing the common velocity to zero.

1.7. FWMAV project analysis

Analysing the different FWMAVs developed over the last two decades has provided insight in the different design approaches and more importantly which of these design approaches have shown beter rates of success.

The first important design choice when it comes to FWMAVs is the actuator used for providing the flapping motion of the wings. There are two preferred actuator choices, namely a DC-motor and the piezoelectric actuator. The DC-motor is often used in larger FWMAVs due to its weight. It is sometimes combined with hinged, controlled wings in order to control the orientation angles of the wings. Piezoelectric actuators are more often used in smaller scale FWMAVs due to their relatively small size. In the design of FWMAVs using piezo actuators the design of control is often ignored due to the inability to fit any form of controller with sensors on to the FWMAV, let alone a power source to power it all. Of the 20 projects that were evaluated 15 obtained some form of flight of which 10 were free flight. Of the 10 that obtained free flight 2 were actuated using a piezo actuator.

When it comes to the control of the analysed FWMAV projects there are 6 projects that obtained some form of flight while implementing control. It is interesting to observe that all 6 of these projects use a DC-motor as their actuator, probably due to the fact that the DC-motor allows for larger weight capacity for components such as sensors and controllers. Of the 6 projects with some form of control only the Delfly nimble achieved fully autonomous free flight.

The sensors used in the controlled FWMAVs don't show a clear trend. The most noteworthy sensor used is the stereo vision used by the Delfly nimble which makes use of depth information obtained from two horizontally displaced cameras in order to control the FWMAV. This is the sensor that comes closest to the way optic flow might be used to control the Atalanta.

1.8. Analysis of optic flow and control

As discussed in Section 1.5 optic flow might be used in a range of different methods, however literature has already shown success with some of these methods, namely direct optic flow used by Van Vrede [31] and the use of optic flow divergence used by Ho et. al. [12] in constant divergence landings. The success with these simpler methods suggests that the more advanced methods, proposed in Section 1.6, that require a lot more computing power are more complex than necessary for the control of the Atalanta. Van Vrede [31] showed that direct optic flow can be used to control an FWMAV or quadcopter when combined with simple control. The FWMAV was able to attain a hovering state and move within the room, however close to the walls or during object avoidance this method still becomes unstable. The success of this method combined with the instability close to walls and during object avoidance suggest, that with further improvement of the method it can be used to control the Atalanta, even close to the walls.

Based on the success shown by De Croon using constant divergence as means of controlling the

landing of a FWMAV, an initial study was done in order to investigate the possibility of using divergence optic flow for hover control. The initial study has looked into the possibility of using constant divergence to control the FWMAV and attain a hovering state.

In order to test the possibility of using constant divergence a simple numeric simulation was created. In the model the assumption was made that wings of the atalanta provide a purely translational accaleration and rotations were neglected since they will not have a direct influence on the divergence. Using the initial velocity and position of the Atalanta and the accaleration provided by the wings the state and sensor values of can be calculated. The divergence optic flow values are used in a zero divergence control loop to calculate the accaleration provided by the wings, here the dynamics of the wing are neglected for simplicity. The zero divergence control loop attempts to bring the divergence of both the positive and negative looking sensors to zero. This can be achieved by either bringing the velocity to zero, or by increasing the distance to the wall till infinity. Since increasing the distance to one wall will decrease the distance to the other wall, the control loop should bring the velocity to zero, attaining a hovering state.

Based on different initial conditions the behaviour of the model was analysed, illustrated in Figure 1.4. From Figures 1.4a and 1.4b we can observe that for higher initial velocities it becomes harder for the model to attain hover, resulting in a final position closer to the wall. Here the limiting factors are the control gain and the maximum accaleration of the model. A larger wall to wall distance results in a hovering state further from the wall, as can be seen when comparing Figures 1.4c and 1.4d for the normalized wall to wall distance.

(a) Simulation for multiple initial velocities with a wall distance of 5 meter

(b) Simulation for multiple initial velocities with a wall distance of 10 meter

(c) Simulation for multiple initial velocities normalised for a wall distance of 5 meter

(d) Simulation for multiple initial velocities normalised for a wall distance of 10 meter
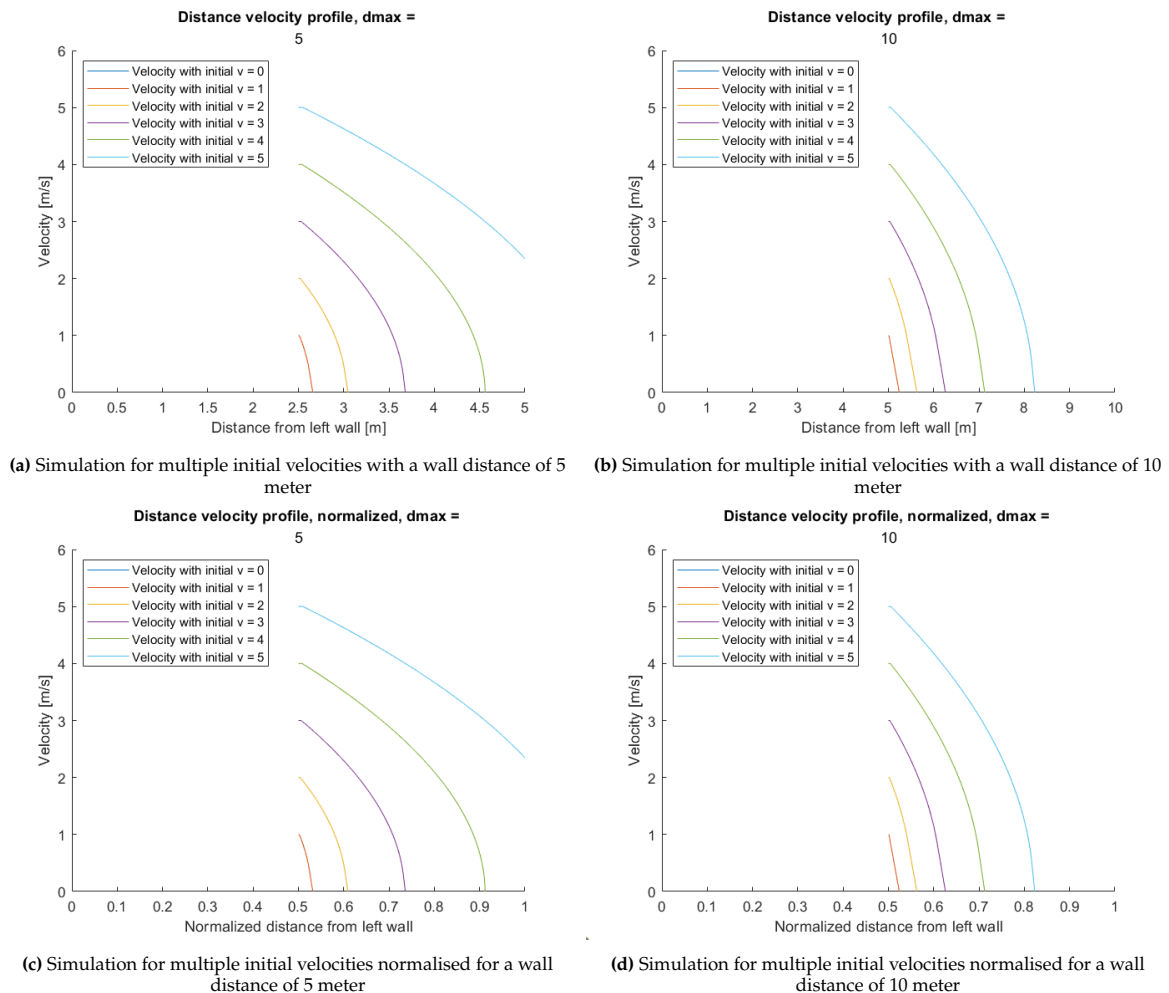
Figure 1.4: Velocity profiles for different initial conditions with 0 divergence control.

1.9. Project description

Based on the analysis of the state of the art and literature it can be observed that a lot of progress can still be made on both the Atalanta and FWMAVs in general. As observed an increasing number of FWMAVs have attained some form of flight, however the increase in controlled flight was less significant. The lack of progress partly originates in the complexity of the control problem with limited computing and power availability. Optic flow might offer an alternative to the stereo vision approach used in the Delfly. As discussed in Section 1.7 literature has shown that it is possible to use optic flow directly to partially control the Atalanta and theory suggest the possible use of divergence optic flow as a method of control. Based on the partial success of direct optic flow and the promise shown by divergence optic flow research questions can be posed in order to guide the further development of the Atalanta FWMAV and its control structure.

- Can a stable hovering state of a FWMAV be obtained using purely optic flow based strategies in an arbitrary environment.

Based on the discussed literature two approaches will be taken in order to answer these research questions, the first approach will look into further developing the direct optic flow control method, while the second approach will focus on the use of divergence optic flow for its control signal.

1.10. Project approach

In order to methodically develop the control algorithms using optic flow, the following steps will be taken:

1. Setup simulation that can be used to test the later developed control loops.

    (a) Develop the dynamics simulation block.
    (b) Develop the sensor block.
    (c) Develop the actuator and aerodynamics block.
    (d) Develop the environmental block.
    (e) Develop the visualisation block.

2. Develop control loop capable of hover using optic flow (both direct and divergence optic flow)
3. Analyse controllers for different initial conditions and environments

First a simulation environment will be developed in which the later developed control loops can be tested, using a dynamic model of the Atalanta. The simulation should be developed in a modular fashion, allowing for the upgrade of different segments of the simulation without largely affecting other blocks. Secondly the control algorithms using both divergence and direct optic flow for a hovering state will be developed. These algorithms will first be tested in order to determine the rate of success and need for further improvement. The decision was made not to include any physical testing in the initial schedule, due to large amount of time needed for the design and setup of the physical test, caused by the fact that the current prototype is not capable of independent flying. A test of the sensors will initially not be made either for the similar reasons, in addition to the fact that in a further design stage a more optimal sensor might be selected.

The focus of the research will be on the development of the control algorithms and on determining the ranges of stability of the system. In the testing stage of the control algorithms extra care will be taken in designing and developing environments and conditions in which the boundaries of stability can be tested.

<div style="text-align: right">

2

Simulation

</div>

This chapter discusses and elaborates on the design and set up of the simulation. It explains how the simulation is structured. It then elaborates on the contents of the most important simulation blocks. Finally, it explains the method of data analysis which serves as bases for the further analysis and comparison of results in later chapters.

2.1. Simulation structure

In order to develop the simulation environment a flow chart was developed in which all relations between the different aspects of the system were displayed as shown in Figure 2.1. This flow chart allows for a modular approach to developing the simulation environment. Each of the blocks within the flowchart can be independently developed based on its in- and outputs without major effects on the simulation as a whole. It further allows for the improvement, alteration and expansion of any give block without compromising the simulation structure. These blocks will all be programmed in Python, where Python was chosen for its versatility and easily usable dynamics libraries. The core of the simulation structure is the dynamics block. In the dynamics block the model is initiated and evaluates the dynamical behaviour of the model for each time step based on the inputs obtained from the other blocks. The dynamics block outputs the state for each time step which can be saved and used for later analysis. The sensor block generates virtual sensor values based on the state of the model using equations described in Section 2.3. Based on the sensor values the controller generates the control signals that should help attain a stable hovering state. The combination of the Actuator and Aerodynamics block generate the applied forces and moments. The generated forces and moments serve as input for the dynamics block which can use the forces the evaluate the next time step. The environmental block contains and initializes all information concerning the information, such as the size and shape of the room. The visualisation block does not concern itself directly with the model and its influences, but serves for the analysis, filtering and saving of simulation data. This block is also used for the post processing of the output data for comparison of different controllers and initial conditions.

2.2. Dynamics

Within the dynamic block of the simulation a method is implemented to accurately evaluate the dynamic behaviour of the Atalanta. A multi body approach, first introduced by Kane [25], was used to simulate the dynamics. This approach models the system as a set of bodies with connecting equations, allowing for the modelling of complex systems. Using a set of generalized coordinates and speeds to simplify the description to a minimum number of independent variables makes it possible to set up a minimum set of differential equations. By implementing this method into Python it is possible to solve the obtained set of differential equations using the numeric solver from the scipy library. Using the numeric solver it is possible to generate the time behaviour of the Atalanta for a given set of initial conditions and time series. In this model the Atalanta is modeled as a single body, with a mass and moments of inertia. The wings are modeled not as separate bodied, but simply as forces exerted on the body at a position corresponding to the wing position. The choice was made to model the wings as simple forces since the mass of the wings is relatively small compared to that of the body.
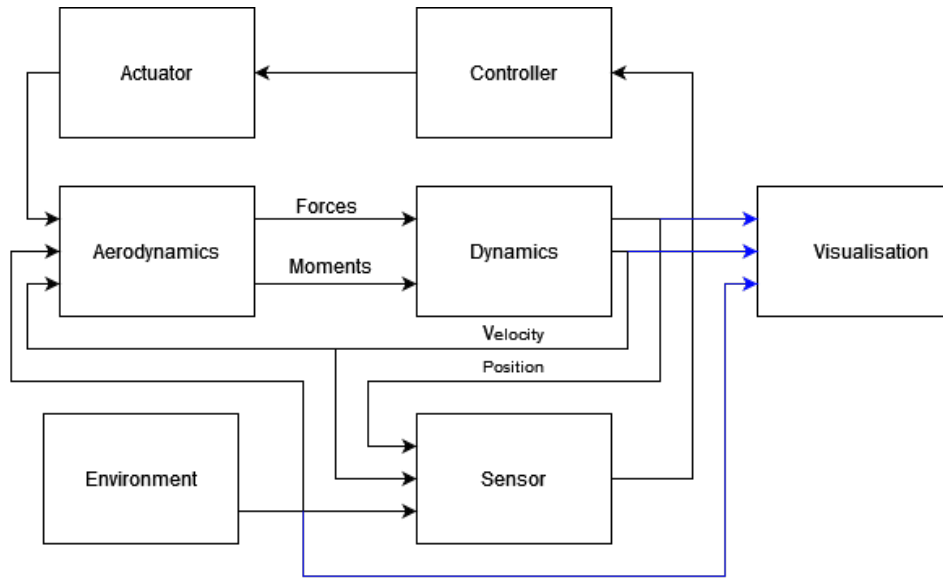
Figure 2.1: The structure of the simulation of the behaviour of the atalanta.

2.3. Sensor evaluation

In order to effectively simulate the behaviour of the Atalanta a mathematical equivalent of the sensors was created for both direct & divergence and curl optic flow sensors. These mathematical equivalents generate the outputs of the sensors based on the velocity and position relative to the walls. These mathematical sensors do not incorporate the image-decay caused by the fact that for most of the time the wall is not exactly at the focal distance, but rather out of focus. The effects of optics in the simulation has not been taking into account, due to the highly complex relations between focus distance, field of view, blur, and optic flow. When it comes to the effect of the field of view it is mostly present at large distances, where the effective area coverage is large. The field of view affects the signal intensity inversely, where a larger field of view results in a lower optic flow signal. It also has a significant effect on optic flow while looking into the corner between two or more connecting walls or bodies, due the effects the different surface angles with respect to the sensor. At large distances the optic flow signals in both direct and divergence approaches are relatively small. A 0 degree field of view was used, since it allows for mathematical simplifications. This simplification allows for the modeling of the sensor with a single line of sight instead of a field of view which has to take into account the intersection between walls. In Section 4.2 the simple sensor description will no longer hold, as the sensor will be modelled more realistically in order to analyse the effect on the behaviour.

2.3.1. Direct optic flow sensor

The direct optic flow sensor takes the sum of the optic flow vector field in the two principle directions resulting in two sensor values, one along the horizontal and the other along the vertical axis. The resulting in values indicating the effective motion along the vector surface. Based on this description the direct optic flow in 3D can be simplified using vector equations. First the general velocity vector $\vec{v}$ is projected onto the sensor surface along the principle axis of the sensor $\vec{r}_{p1}$ and $\vec{r}_{p2}$ using Equation 2.1. Here $\vec{r}_{p1}$ and $\vec{r}_{p2}$ lay within the sensor plane and are parallel to two of the local axis, x, y and z and perpendicular to I^+. This results in the effective velocity of the sensor $\vec{v}^{I^+}_{p1,sens}$, if the observed wall were parallel to the sensor surface belonging to the I^+ facing sensor. Where I^+ is the direction of the sensor aligned with one of the local axis, x, y and z. The velocity projections on the sensor are then projected onto the wall using Equations 2.2 and 2.3, accounting for the angle of the wall and its effect on the optic flow field. Here $\vec{s}_{p1}$ is the projection of the principle axis onto the wall surface and $\vec{w}_1$ is the vector perpendicular to the wall surface used to describe the wall. Furthermore $\vec{v}^{I^+}_{p1}$ is the projection of the velocity onto the sensor accounting for a non parallel wall. Combining these equations with the description of optic flow behaviour results in Equation 2.4, where $OF^{X^+}_z$ is the optic flow in z direction

as observed by the X^+ looking sensor, r^{X^+} is the distance to the wall, $\vec{\omega}_y^{X^+}$ the rotational velocity of the X^+ facing sensor around the y axis and $f^{X^+}(\psi, \theta, \phi)$ a function accounting for field of view and other sensor factors. It is important to note here that in Equation 2.4 the + signs may change to − signs dependent on the facing direction and observed principle axis.

$$\vec{v}_{p1,sens}^{I^+} = (\vec{r}_{p1} \cdot \vec{v}) \cdot \vec{r}_{p1}, \tag{2.1}$$

$$\vec{s}_{p1} = \vec{w}_1 \times \vec{r}_{p1} \times \vec{w}_1, \tag{2.2}$$

$$v_{p1}^{I^+} = \frac{\vec{v}_{p1sens} \cdot \vec{s}_{p1}}{|\vec{s}_{p1}|}|, \tag{2.3}$$

$$OF_z^{X^+} = \frac{v_z^{X^+}}{r^{X^+}} \cdot f^{X^+}(\psi, \theta, \phi) + \omega_y^{X^+}. \tag{2.4}$$
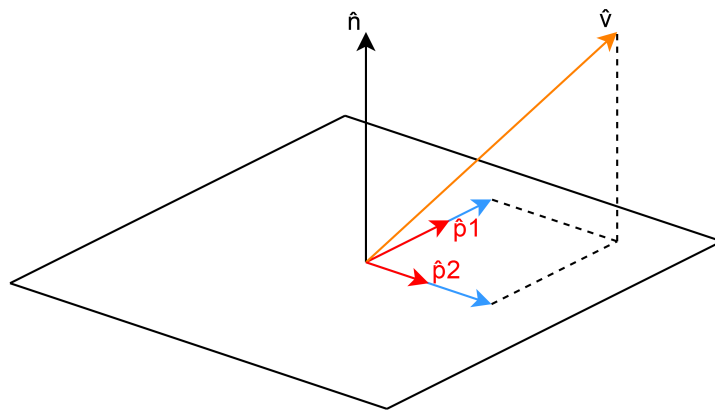

Figure 2.2: Visualisation of the projection of the velocity onto the sensor surface.
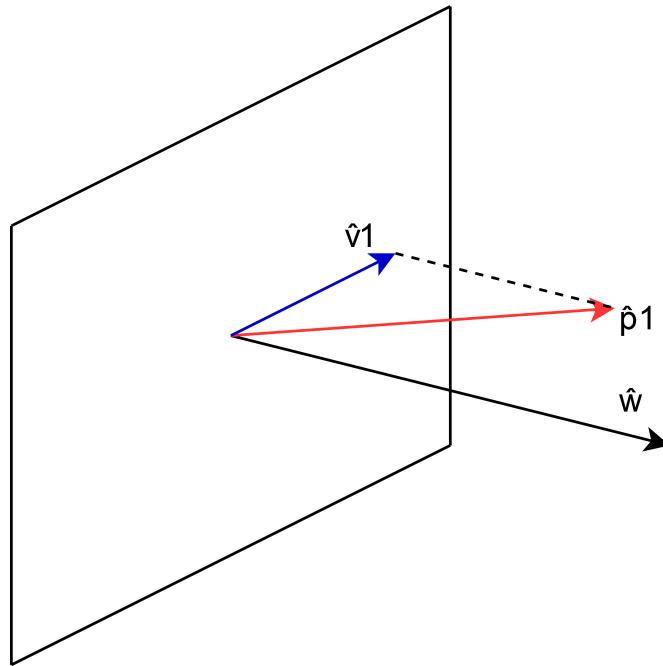

Figure 2.3: Visualisation of the projection of the velocity onto the wall surface.

2.3.2. Divergence and curl optic flow sensor

Opposed to the direct optic flow sensor, the divergence and curl optic flow sensor use the optic flow behaviour at the border or along a given closed trajectory. The divergence flow is given as the optic flow that moves out of the field of view. The curl flow is the complement of the divergence and is the optic flow along the field of view border. The divergence optic flow can be represented by Equations 2.5 and 2.6, where they respectively represent the divergence and curl of the optic flow field. In Equation 2.5 D^{X^+} is the divergence optic flow of the X^+ facing sensor. Here v_x is the velocity in the X^+ direction and r^{X^+} the distance to the wall in that same direction. In Equation 2.6, C^{X^+} is the curl simply given by $\omega_y^{X^+}$, the rotational velocity of the X^+ facing sensor around the y axis.

$$D^{X^+} = \frac{v_x}{r^{X^+}} \cdot f^{X^+}(\psi, \theta, \phi), \tag{2.5}$$

$$C^{X^+} = \omega_y^{X^+}. \tag{2.6}$$

2.4. Data analysis

The goal is to analyse the effect of different initial conditions on the behaviour of the two different controllers. This calls for the need to effectively and efficiently compare multiple initial conditions, since the data that is generated by the simulated model consists of time series and the corresponding states. The states consist of 3 translational and 3 rotational coordinates and 3 translational and 3 rotational velocities, resulting in a data set for 12 variables and a matching time series. The most important information that can be obtained from this dataset is the trend over time for each of the variables. The trend of the behaviour will give an indication whether a stable hovering state might be obtained. Since comparing each variable with the matching one for every simulation is very time consuming, an efficient method is needed to compare the results of different simulations with each other. Since the focus is on the stability of the controllers for different initial conditions, the general behaviour of the motion is of more interest compared to the high frequency behaviour. The general behaviour of the system is dominated by a decay function whereas the high frequency behaviour is dominated by an oscillatory function. Since interest is mostly focused on the general behaviour it is possible to compare only the general decay of each simulation instead of the high frequency oscillatory behaviour. In order to obtain a measure of the decay an exponentially decaying curve is fitted across the tops of the oscillatory motion as shown in Figure 2.4. The curve fit is described by Equation 2.7, here λ represents the decay factor of the function, A is a measure of the amplitude and c is an added constant to compensate possible offsets. The decay factor allows for the relatively easy comparison of different initial conditions and their general behaviour, since they are not dependent on the frequency, amplitude or offset of the behaviour.

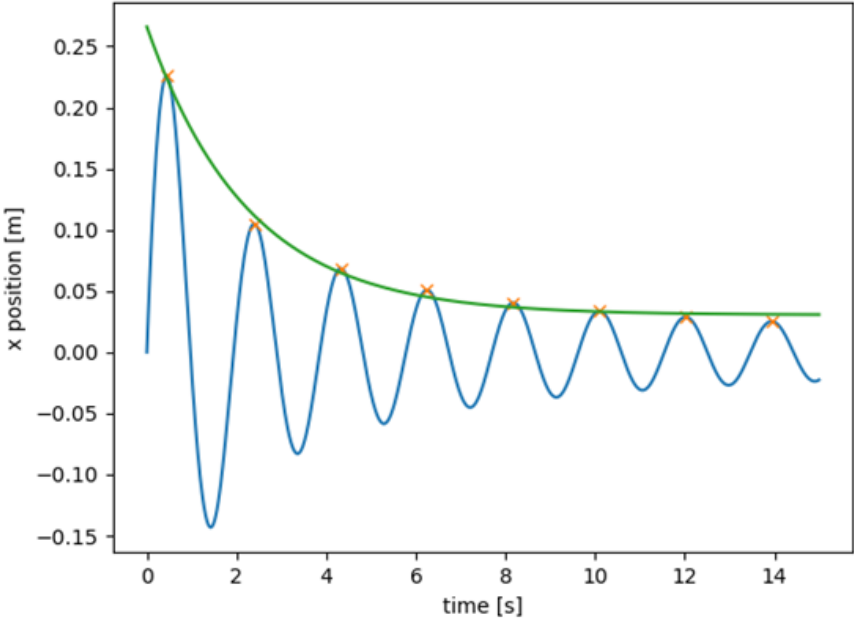$$f(t) = A \cdot e^{\lambda \cdot t} + c. \tag{2.7}$$

Figure 2.4: Curve fit across simple data.

3

Controller design

In order to effectively design the controller, control theory is used to estimate some of the broad limits of the controller determined by the physics of the system. Based on the broad limits a general method is designed which can be modified to fit the different sensor types. After, the general method is modified to fit either the direct or divergence and curl sensors.

3.1. Control theory

Within control theory it is possible to determine the theoretical maximum of the sensors and control. First the observability and limits of the sensors are discussed for both types of sensors. Afterwards the controlability for the given wings are discussed which concerns the states which can be obtained.

3.1.1. Observability

Before a general control approach can be formulated it is important to first analyse the observability of the system in order to determine which parts of the state of the Atalanta can be observed during operation. A standard matrix approach to observability is not possible for this system due to combination of the complex nonlinearities in the system and the fact that the general dynamics are formulated within the simulation. However, based on the equations it can be argued whether the system is observable for either direct of divergence optic flow

Direct observability
When analysing Equation 2.4 it can be determined that there are 12 sensor values which can provide insight into the systems state. On the other hand there are a large number of unknown variables namely, 6 velocities and 6 angular velocities, 6 wall to sensor distances, 3 system angles and 6 wall to sensor angles. Resulting in a total of 27 unknown variables. Having only 12 equations and 27 unknowns the system can never be observable. It is important to note that it therefore is not possible to extract the exact value of any of the desired variables which in this case are the velocities and angular velocities. It is possible to determine an estimate of the desired variables by the simple addition and subtraction of a subset of the 12 equations. Resulting in a set of 6 variable estimations, 3 which represent the estimated velocities of which Equation 3.1 represents the velocity in i direction using sensor data from the different direction facing sensors. The other 3 equations represent the estimated angular velocity for which Equation 3.2 represents the angular velocity around the i axis. Here i represents a single local axis x, y or z, while j and k represent their right handed complements. Within these equations I^+, I^-, J^+, J^-, K^+ and K^- represent either the positive or negative facing sensors along their corresponding axis i, j and k.

$$v_i = \frac{1}{2} \cdot \left(\frac{v_i^{J^+}}{r^{J^+}} \cdot f^{J^+}(\psi, \theta, \phi) + \omega_k^{J^+} + \frac{v_i^{J^-}}{r^{J^-}} \cdot f^{J^-}(\psi, \theta, \phi) - \omega_k^{J^-} + \frac{v_i^{K^+}}{r^{K^+}} \cdot f^{Z^+}(\psi, \theta, \phi) + \omega_j^{K^+} \frac{v_i^{K^-}}{r^{K^-}} \cdot f^{K^-}(\psi, \theta, \phi) - \omega_j^{K^-} \right).$$

(3.1)

$$w_i = \frac{1}{2} \cdot (\frac{v_j^{K^+}}{r^{K^+}} \cdot f^{K^+}(\psi,\theta,\phi) + \omega_i^{K^+} - \frac{v_j^{K^-}}{r^{K^-}} \cdot f^{K^-}(\psi,\theta,\phi) + \omega_i^{K^-} + \frac{v_k^{J^+}}{r^{J^+}} * f^{J^+}(\psi,\theta,\phi) + \omega_i^{J^+} - \frac{v_k^{J^-}}{r^{J^-}} \cdot f^{J^-}(\psi,\theta,\phi) + \omega_i^{J^-}).$$

(3.2)

Divergence observability

In the case of divergence, opposed to direct optic flow, it can be observed from Equations 2.5 and 2.6 that the divergence and curl contain different terms allowing for the easier separation of terms even though the same number of unknowns are present in the equations. The 6 curl terms allow for a simple determination of the angular velocity term described by Equation 3.4. The divergence equation still contains the distance and angle terms allowing only for the estimation of the velocity using Equation 3.3. These equations use the same definition for i, I^+ and I^- as those used in Equations 3.1and 3.2, but instead of using direct optic flow equations using the divergence and curl optic flow equations.

$$v_i = \frac{\frac{v_i^{I^+}}{r^{I^+}} \cdot f^{I^+}(\psi,\theta,\phi) + \frac{v_i^{I^-}}{r^{I^+}} \cdot f^{I^-}(\psi,\theta,\phi)}{2},$$

(3.3)

$$w_i = \frac{\omega_i^{I^+} + \omega_i^{I^-}}{2}.$$

(3.4)

3.1.2. Controlability

Similar to observability, the nonlinearities within the system do not allow for the determination of the controlability of the system, however based on the knowledge of the actuation mechanism and the general behaviour of the system we can make some predictions on the controlability of the system and whether a state can stability be attained.

First, it is important to note that there are four off center wings providing a pure vertical force on average during a single flap. This allows the system to pitch and roll by selectively increasing and decreasing thrust in each of the wings. When the system is not perfectly vertical it will always start moving in a horizontal direction, this means that any state in which the pitch and roll angle can not be attained stably only momentarily either during horizontal motion or rotation. Furthermore, when the pitch or roll angle becomes to large the direction of actuation will partially align with the direction of gravity making it an unrealistic state to attain. When gravity is aligned with the direction of actuation a crash to the ground is highly likely since rotation back against gravity is always associated with an acceleration towards the ground. It is however possible to attain any realistic horizontal and vertical position since a horizontal translation is an inherent consequence of changing angle and gravity can be used to accelerate towards the ground while in a vertical position. Lastly, it is possible to control the yaw angle of the system by first pitching, then rolling and then pitching and rolling back upwards towards vertical alignment, however since there are sensors present in each of the 6 principle directions and movement is possible in any direction within the horizontal plane it is not strictly necessary to control the yaw angle.

3.2. General approach

Optic flow in both approaches provides some relation following velocity over distance and angular velocity. Both the direct and divergence method aim to decrease the velocity along and angular velocity around each of the axes. The velocity can be decreased by tilting the FWMAV counter to the velocity, by decreasing the thrust of the back two wings and increasing thrust on the front two wings. The angular velocity can be decreased by generating a moment around the same rotational axis by decreasing thrust on one side of the FWMAV and increasing thrust on the other side. If these principles are to be used for the stable control of the Atalanta the rotational and translational terms need to be separated as much as possible. Using the separated terms a general control method is devised based on the previously discussed approaches for decreasing velocity. For each of the four wings this results in an variation of Equation 3.5 where only the signs change depending on the positioning the wings relative to the sensors. Term 1 ensures the compensation of gravity when no sensor signals are present. Terms 2, 3 and

5 aim to compensate respectively the z, x and y translational velocity. The last terms, namely 4 and 6 attempt to decrease the angular velocity around the y and x axes respectively.

Based on Equations 3.1 and 3.3 it is possible to observe that the direct and divergence method are each others complement. For the velocity in the x direction the direct method contains sensor values from the sensors perpendicular to this direction of motion, namely y and z facing sensors. For the same velocity in x direction the divergence method takes the sensor values in the x direction. This results in the fact that divergence with the x direction and direct with y and z form a independent set of sensors and can therefore be seen as each others compliment.

$$C = \underbrace{1}_{1} - \underbrace{g_{trans} \cdot (v_z)}_{2} \pm \underbrace{(g_{trans} \cdot (v_x) - g_{rot} \cdot (\omega_y))}_{3 \qquad 4} \pm \underbrace{(g_{trans} \cdot v_y - g_{rot} \cdot (\omega_x))}_{5 \qquad 6}. \tag{3.5}$$

3.3. Direct optic flow

The first method for control using optic flow is based on the control model suggested by Goosen [9]. The proposed controller makes use of optic flow signals obtained from the 6 sensors facing the different principle directions. Each sensor puts out two signals corresponding to the velocity along the sensor surface. This means that the sensor does not observe the velocity in the direction the sensor is facing, but perpendicular to this facing direction.

In the case of direct optic flow Equations 2.4 can be used to obtain the estimate of the translational en rotational velocity terms as described in Section 3.1. The substitution of variations of Equations 3.1 and 3.2 into Equation 3.6 result in a controller that might be capable of stable control of the Atalanta. Here C_{w_1} indicates that it is the control signal for wing 1.

$$C_{w_1} = 1 - g_{trans} \cdot (v_z) + (g_{trans} \cdot (v_x) - g_{rot} \cdot (\omega_{y_x} - \omega_{y_z})) + (g_{trans} \cdot v_y - g_{rot} \cdot (\omega_{x_y} - \omega_{x_z})). \tag{3.6}$$

3.4. Divergence and curl optic flow

For the controller using divergence and curl information the approach is more straightforward. The divergence gives an estimate of the velocity over distance in the direction of the sensor. The direction and magnitude of the in a given direction are obtained by taking the difference between the two divergence sensor values along that direction. Similarly an estimate of the rotation direction and magnitude are obtained by summing the curl sensor values around the given axis. It is important that the magnitude here not only represents part of the velocity but also the distance to the wall, allowing for stronger corrections close to the wall and at high speeds when implemented correctly. Using the aforementioned estimates a controller is developed that attempts to minimize all signals simultaneously in attempt to obtain a hover state, by using the approach as described in Section 3.2. This results in the following control signal equations for the different wings. The equation for wing 1 is given in Equation 3.7. In Chapter 4 the divergence controller will be compared to the direct controller for different gain magnitudes and ratios, as well as for different initial conditions and sensor descriptions.

$$C_{w_1} = 1 - g_{trans} \cdot (v_z) + (g_{trans} \cdot (v_x) - g_{rot} \cdot (\omega_y)) + (g_{trans} \cdot v_y - g_{rot} \cdot (\omega_x)). \tag{3.7}$$

4

Hover

This chapter discusses and analyses the results of different simulation sets and the effect of different conditions on the behaviour. It first starts with different cases for the ideal sensors. For the ideal sensors a large number of different cases are discussed and analysed. It then looks at the non-ideal variation of the sensor and analyses the effect of this non-ideal sensor on the basic behaviour of the system in order to draw conclusions on its influence.

4.1. Ideal hover

This section will compare the effect of different parameters on the behaviour of the Atalanta within the simulation. First the general initial conditions such as position and velocity are studied. The effect of different gains within the controller is then studied in order to analyse how gain affects the stability of the system.

4.1.1. Initial conditions

The initial conditions of the ideal sensor can be split up four different groups, which each have their own separate influence on the behaviour of the system. These groups have been analysed separately, for a unity gain, in order to distinguish the individual effects of each of these condition groups. The effect of combinations is not explicitly studied, due to the time and data complexity being O^n while providing only insight into the specific case. First the initial position is analysed, concerning itself with the initial x, y and z position of the system. Then the effect of different pitch and roll angles is studied before analysing the effect of the size and shape of the room on the behaviour. Lastly the effect of the initial velocity on the behaviour is studied.

Initial position

When analysing the initial conditions the most important initial condition is the position from which the analysis starts. The initial position may affect the initial sensor values and therefore the further sensor and control values. When it comes to the effect of the initial positions on the control some general predictions can be made. Based on the control equations and sensor dynamics the expectation is that the direct control is affected by an off center position that is not along the axis of initial velocity. For the divergence control the opposite should be true, an off center position along the axis of motion will affect the control behaviour.

   In this analysis the initial position ranges from -0.8 times the room size till 0.8 times the room size along both the x and z axis. In order to model both parallel and perpendicular initial velocities the initial velocity has been simulated for a case both along the x and y axis.

(a) Initial velocity in the x direction.

(b) Initial velocity in the y direction.
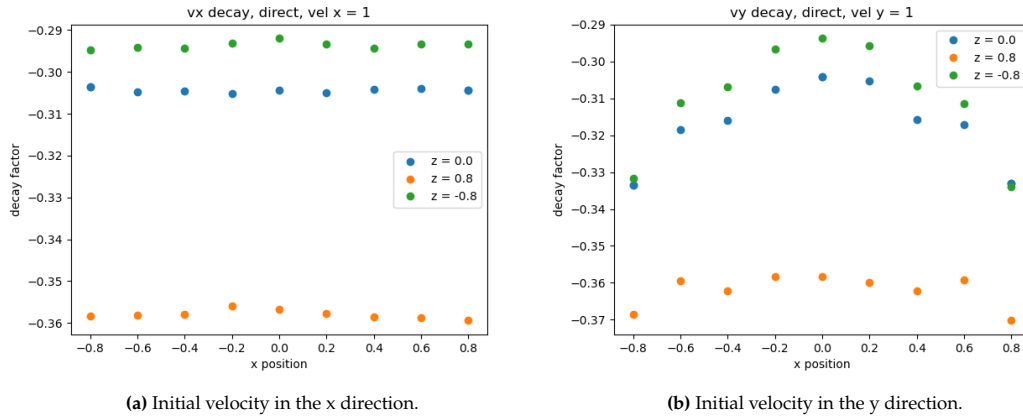
Figure 4.1: The effect of height and normalised horizontal position on decay for the direct controller for different initial velocities.

(a) Initial velocity in the x direction.

(b) Initial velocity in the y direction, note here the small y-axis.
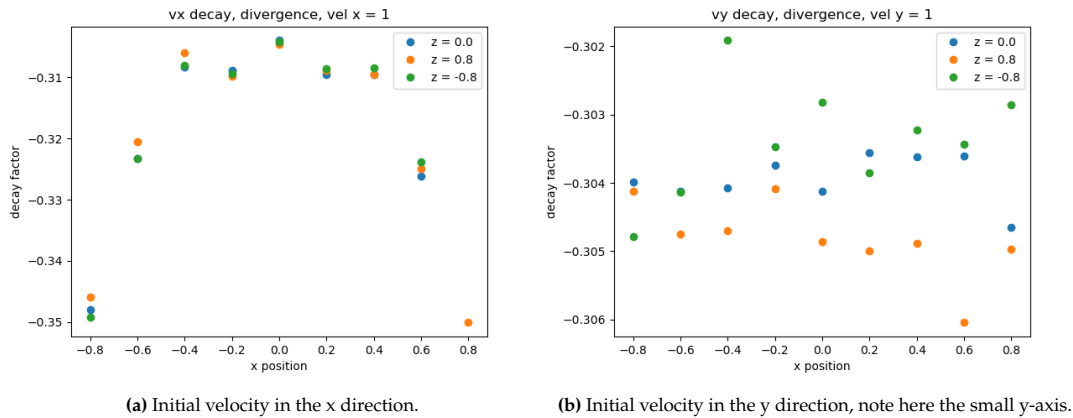
Figure 4.2: The effect of height and horizontal position on decay for a divergence controller for different initial velocities.

The first case that is analysed consists of a simulation run at three different heights, namely a factor 0.8, 0 and -0.8 from the center of the room to the ceiling. For each of these three cases the simulation is run for a set of different horizontal positions along the x axis. The position along the x axis ranges from a factor of 0.8 to -0.8 from the center to the wall in increments of 0.2. This set of simulations is first run for the developed direct controller. The results for the two different initial velocities are displayed in Figure 4.1. When looking at Figure 4.1a, where the initial velocity is directed along the x axis, it can be observed that changing the horizontal position in the direction of motion does not directly affect the decay of the system, where changing the height has a significant effect on the decay behaviour of the system. When changing the velocity to be parallel to the y axis instead the result can be observed in Figure 4.1b. For the simulation where the velocity is parallel to the y axis it can be observed that changing the initial position along the x axis does have a significant effect on the behaviour of the system. The results of the simulations correspond to the previously described expected behaviour and the effect of initial position on the behaviour. These results stem from the fact that the direct controller observes the motion with the sensors perpendicular to the direction of motion, which results in the fact that distance changes perpendicular to the direction of motion have a direct influence on the behaviour.

The same set of simulations can be done for the developed divergence controller. The results for the divergence controller can be observed in Figure 4.2. The behaviour of the divergence controller, opposed to the direct controller, is not affected by a change in the z direction. The behaviour is affected by the change in the position along the x axis when the velocity is parallel to the x axis as shown in Figure 4.1a, but is not affected by the same change when the initial velocity is directed along the y axis. These results also match with the predicted behaviour. It is also important to note that opposed to the direct controller, the divergence controller does not experience any significant effect of height on the decay

behaviour. This originates from the fact that the divergence controller only observe distance changes in the direction of motion, while the direct controller observes them perpendicular to the direction of motion.

(a) Initial velocity in the x direction.

(b) Initial velocity in the y direction.
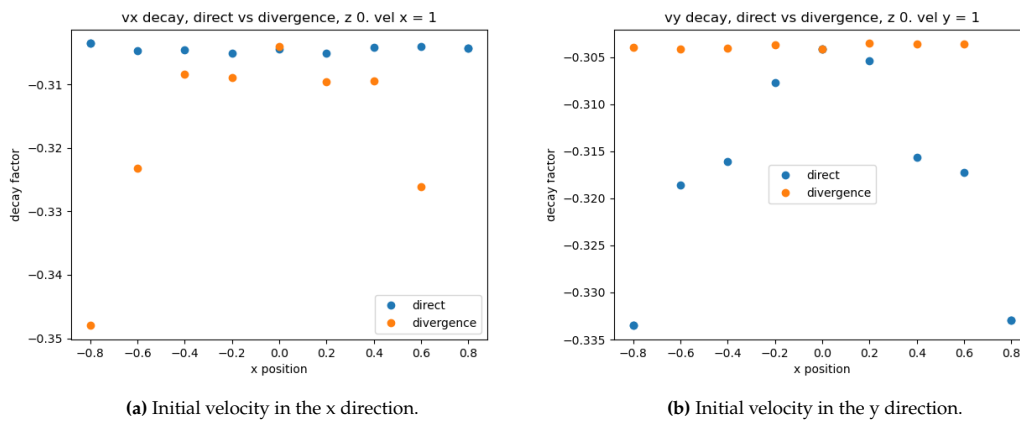
Figure 4.3: Comparison between the direct and divergence controller for different initial velocities and x positions where z = 0.

Having observed the effect of different initial conditions on the different controllers, it is possible to compare the two controllers using Figure 4.3. In Figure 4.3 the two different controllers match in their behaviour when they are centered. When comparing Figure 4.3a with Figure 4.3b it can be noted that the behaviour of divergence for a velocity along the x axis is very similar to the behaviour of direct for a velocity along the y axis. This behaviour is expected since the method of both controllers is the same, but sensors effects present are each others complement as discussed in Section 3.2.

Initial angle
Not only the initial position is of importance, but so is the initial angle in which the system starts. During operation a case may present itself in which the system is flying with an angle or slightly tilted during hover which result in a non zero initial angle with a possible non zero velocity. The effect of these initial conditions are shown in Figure 4.4. When analysing the figures it can be seen that there is an effect of the initial angle on the decay of the system. The most important thing to note is that when no initial velocity is present an initial angle will cause the system to start oscillating resulting in a non zero decay factor. The second interesting thing to note is the fact that in most cases the system decays faster when an initial velocity is present, possibly due to the stronger control singles allowing for a stronger correction of the undesired behaviours.
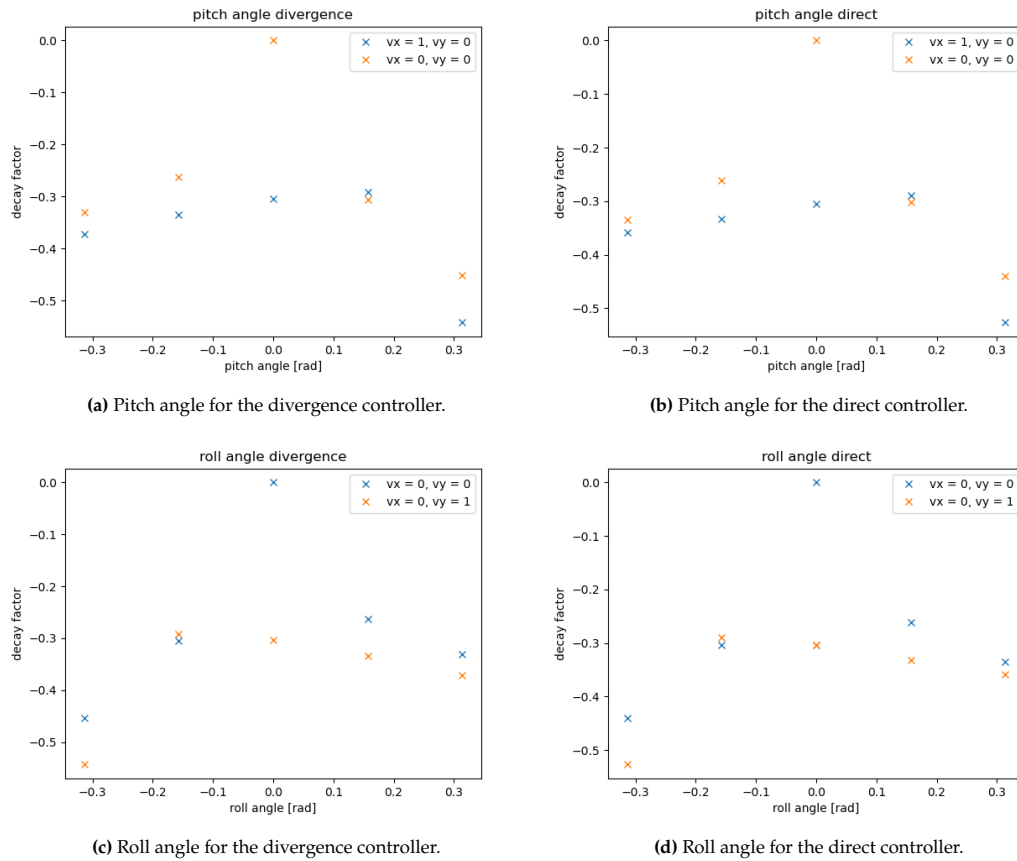
(a) Pitch angle for the divergence controller.

(b) Pitch angle for the direct controller.

(c) Roll angle for the divergence controller.

(d) Roll angle for the direct controller.

Figure 4.4: Effect of different initial velocities and initial pitch or roll angle on the behaviour of the two controllers.

Room dimensions

It is not only important to analyse the effects of the initial position within a given room, but also the effect of the different room dimensions on the behaviour. For this reason the same simulation set was run for different room dimensions, namely rooms of (Lx, Ly, Lz) is (2, 2, 2), (2, 2, 4), (4, 4, 2) and (4, 4, 4) meter. Based on the effects observed in Section 4.1.1 some predictions can be made on the expected behaviour of both the direct and divergence controller. For the direct controller it is expected that any change in room size will have some matter of effect on the behaviour of the controller. For divergence controller it expected that only changes in the direction of motion affect the behaviour of the controller.

(a) decay and velocity in x direction.

(b) decay and velocity in y direction.

(c) decay in z and velocity in x direction.

(d) decay in z and velocity in y direction.
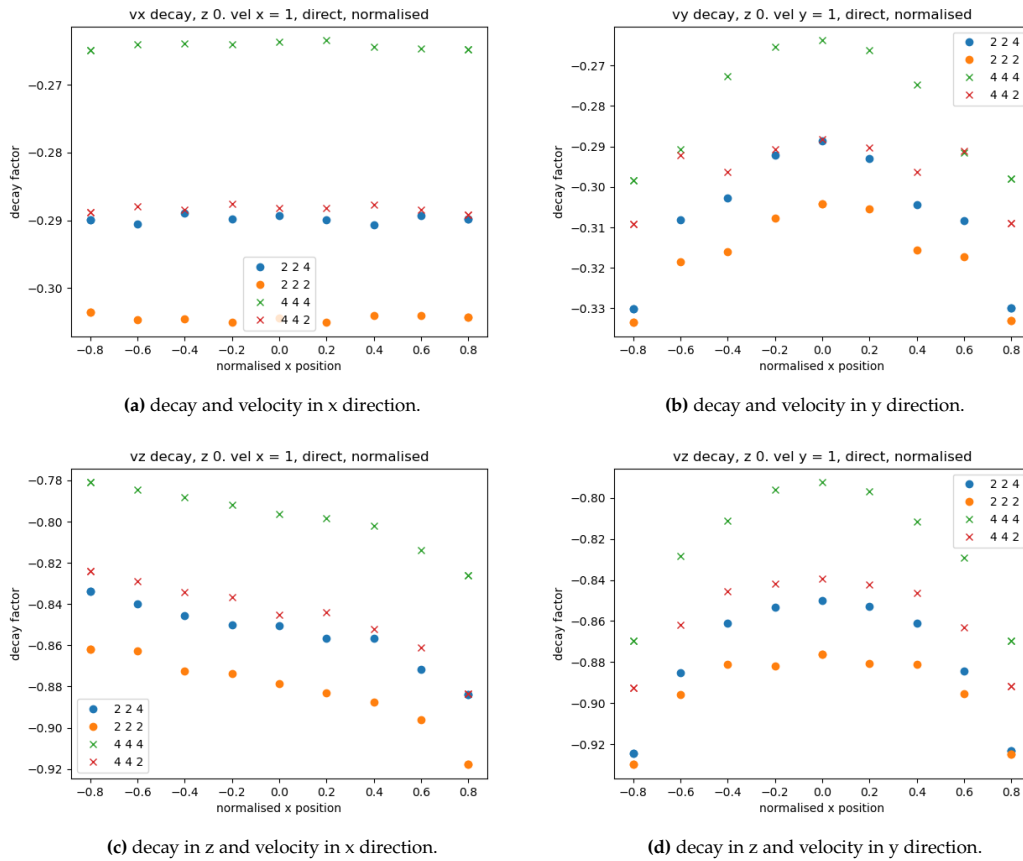
Figure 4.5: Effect of different room sizes on the behaviour of the direct controller for different initial positions and decay directions. The legend shows the x, y and z dimensions of the room from left to right.

For the direct controller it can be concluded from Figure 4.5 that the predictions fit the simulation results. The most important observation is that any change in room size does indeed influence the decay of the system. It is important to note here that the different room size does not significantly impact the shape of the behaviour exhibited. This suggests that the size and shape of the room only affect the magnitude, and possibly frequency, of the behaviour opposed to the inherent behaviour of the controller.

(a) Decay and velocity in x direction.

(b) Decay and velocity in y direction.

(c) Decay in z and velocity in x direction.

**(d)** Decay in z and velocity in y direction.
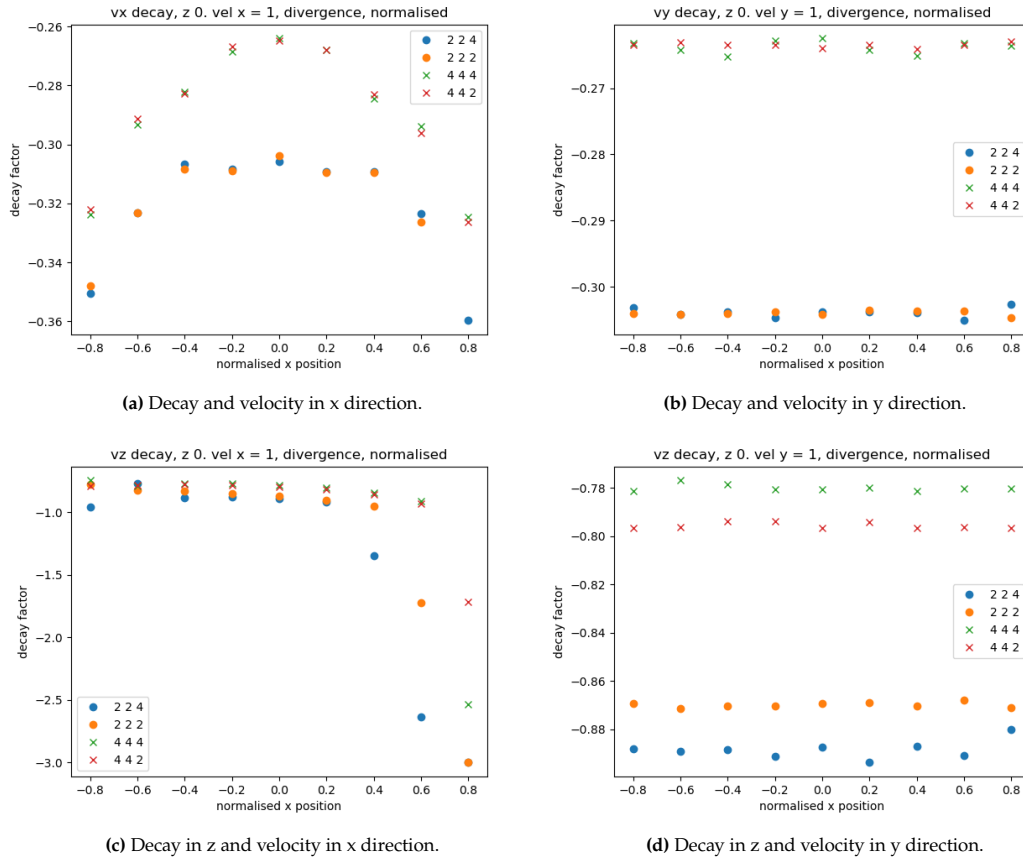
Figure 4.6: Effect of different room sizes on the behaviour of the divergence controller for different initial positions and decay directions. The legend shows the x, y and z dimensions of the room from left to right.
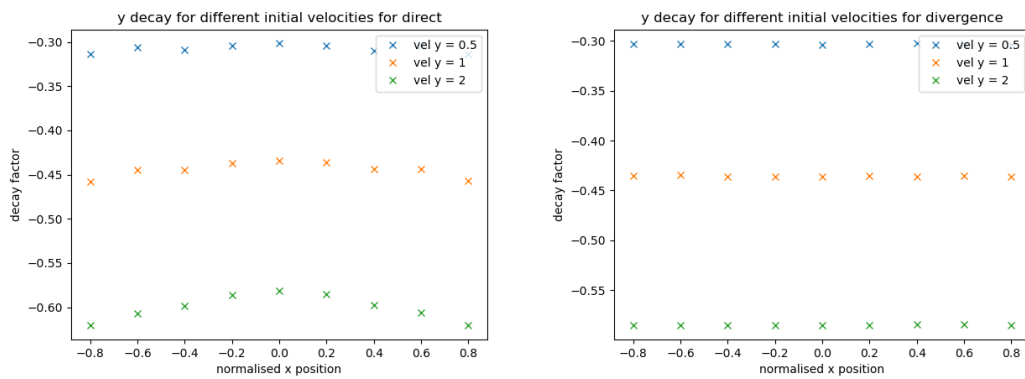
The behaviour of the divergence fits the predictions similarly well. It can be seen that in Figures 4.6a and 4.6b that results for which only height has changed are almost perfectly the same as the version with the original height. The z decay does not fit these predictions. In Figure 4.6c and 4.6d it can be seen that no data sets exhibit the same behaviour pattern. This can be explained by the fact that motion in the z direction is influenced by the decay behaviour in the x and y direction. Thus if the behaviour in the x or y direction was already altered by the change in room size, as previously discussed, now the change in z direction will further affect the behaviour. This causes that any change in room size will affect the behaviour in the z direction, which was not accounted for in the prediction of the behaviour.

Initial velocity
The effect of the initial velocity on the behaviour of the Atalanta is more predictable than that of position, angle or room size, since it is only linearly present in the control signal. This means that a higher initial velocity will result in a higher control signal. This simple relation suggests that a higher initial velocity will result in the same behaviour, but with a higher decay for higher initial velocities. Looking at Figures 4.7 show that the simulations fit the predicted behaviour, a larger velocity does indeed result in a higher decay. Similarly a smaller initial velocity results in a smaller decay value. When looking at Figure 4.11 it can also be seen that for a given initial condition the initial velocity only affects the amplitude and decay of the behaviour, but not the frequency. In Figure 4.7b it should be noted that at the position of 0.8 there is no data point present for the highest initial velocity. The absence of this data point is due to the inability of the solver to generate a data output due to a premature stop. The premature stop is in turn caused by need for the solver to take an infinitely small time step since when the simulation (almost) crashes into a wall. The fact that a crash (almost) occurs can be extrapolated based on Figure 4.8 in which it can be seen that for a position of 0.6 the simulated model already comes close to the wall. This behaviour does not occur on the negative side the positions, since the velocity is directed in the positive x direction and it thus moves away from the wall in the negative x direction.
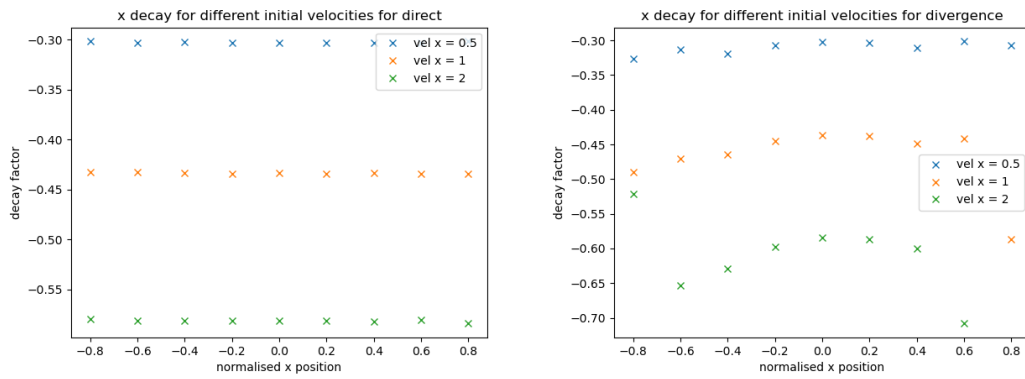
(a) Decay for different initial x velocities on a direct controller.

(b) Decay for different initial x velocities on a divergence controller.

(c) Decay for different initial y velocities on a direct controller.

(d) Decay for different initial y velocities on a divergence controller.

Figure 4.7: Study of the effect of initial velocity on the behaviour of the different controllers for different initial positions
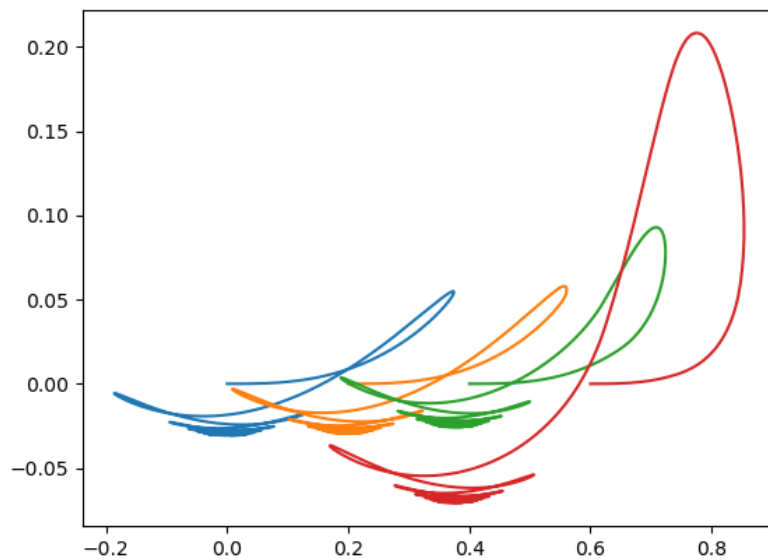

Figure 4.8: Time behaviour for different x positions given a high initial velocity for the divergence controller.

4.1.2. Gain analysis

It is not only important to study the various effects of the different initial conditions on the behaviour of the controller, but it is also important to analyse how different gain factors influence the behaviour. In attempt to gain full insight into the controller the simulation is run for a set of different gain factors for both the translational and rotational term. Based on the results of the initial set, the set is expended in the direction of a larger decay factor. The results of this expended simulation set can be seen in Figure 4.12. In Figure 4.12a it can be seen that all data sets have the same amount of data points, this means that all simulations remained stable for all low rotational and high translational gains. For the divergence controller this is not the case, it can be seen in Figure 4.12b that some data sets are missing data points. The missing data points originate in the fact that the curve fit, which determines the decay factor as discussed in Section 2.4, is unable to determine a curve fit and decay factor for unstable results. This also results in the outlier in Figure 4.12b. When comparing the divergence and direct method it can be seen that both methods show the same trend when it comes to an increasing decay factor. Both an increase in the translational and decrease in rotational gain result in a more desirable decay factor. This behaviour can be explained by analysing the general controller described by Equation 3.5. The goal of controller is to bring both the rotational and foremost the translational motion to zero, since hover is foremost determined by the lack of translational motion and secondly by the lack of rotational motion. When analysing Equation 3.5 there are two important effects based on velocities and gain. The first is the fact that compensation of translational motion also results in a rotational motion since thrust is only generated in the vertical direction relative to the wing. For a larger rotational angle the thrust vector is more aligned with horizontal direction of motion. It is therefore more desirable to have a strong rotational effect for horizontal velocities. The second important thing to observe is the fact that rotational gain helps to decrease rotational velocity. By strongly decreasing rotational velocity using a high rotational gain, only small rotational angles can be obtained. Therefor allowing only small compensation of the translational motion. Based on these two important notes it is logical that a low rotational gain and high translational gain provide more desirable results. The low rotational gain allow for large angles in order to more effectively compensate for translational motion while the large translational gain allows for a faster compensation due to large forces and moments in the desired direction.

It was also studied whether the linear presence of gain could compensate for the linear presence of velocity by studying a set of simulations in which a set of different initial velocities was ran against a set of different rotational and translational gains. The results of these simulations are shown in Figure 4.13, here each colour corresponds to a given initial velocity. It is interesting that, in contradiction with the expectations, initial velocity could not be compensated by a similar factor in gain. This can be seen in the distinct grouping of the different colour sets relatively close together. In order to explain this unexpected behaviour different time responses were shown instead of purely the decay factor this resulted in Figure 4.11 for initial velocity, Figure 4.10 for position and additionally Figure 4.9 for room size. What is interesting to note is the fact that for different initial velocities the magnitude of the motion changes, but the frequency stays the same. For the cases in which different gains and room size are shown it can be seen that it is not only magnitude that changes, but also the frequency of the behaviour. It can furthermore, be noted that in 4.11b the steady state error increase with initial velocity, resulting in a small height loss after during the hovering control.
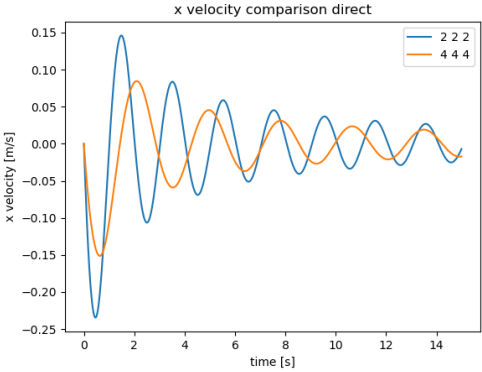
Figure 4.9: Time behaviour of the x position for two different room sizes.
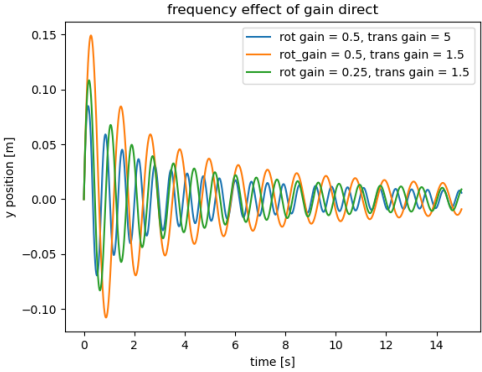
Figure 4.10: Time behaviour of the x position for different controller gains in order to show the effect of controller gain on the behaviour frequency.

(a) Y position time behaviour.

(b) Z position time behaviour.
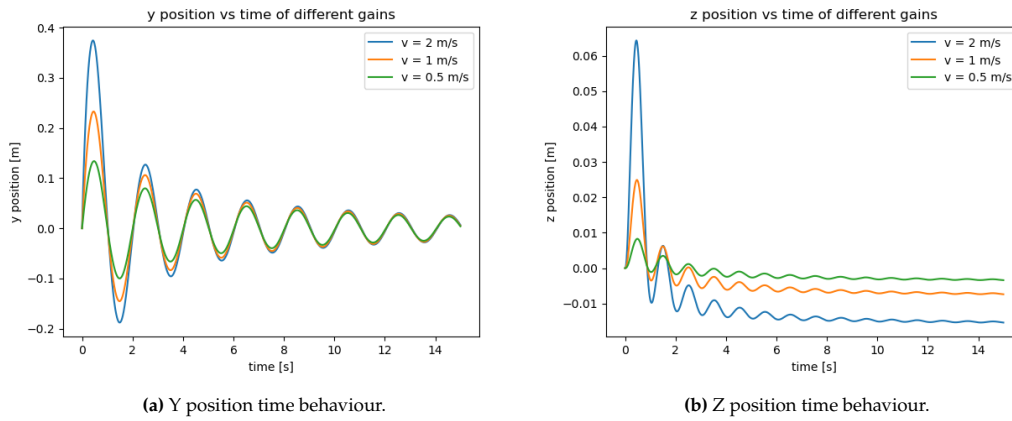
Figure 4.11: Y and z position time behaviour for different initial velocities for the divergence controller.

(a) Direct controller.

(b) Divergence controller.
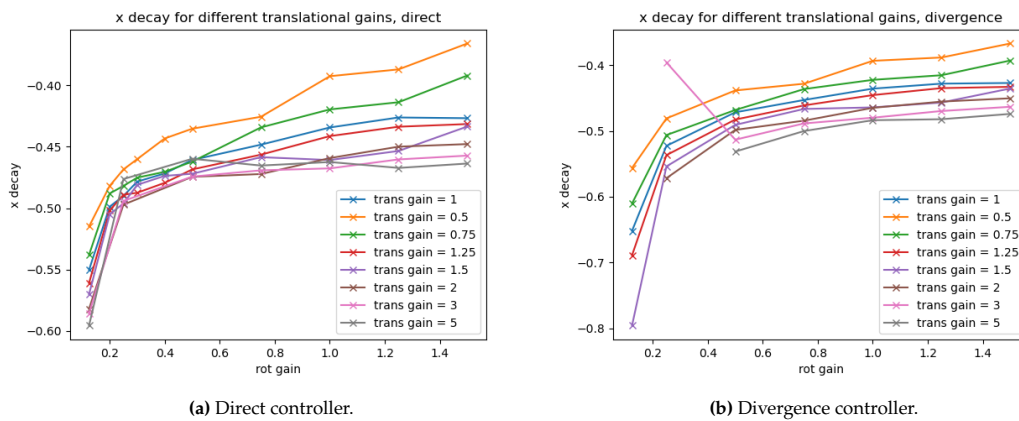
Figure 4.12: X decay factor for different translational and rotational gains and different controllers.

(a) Direct controller.

(b) Divergence controller.
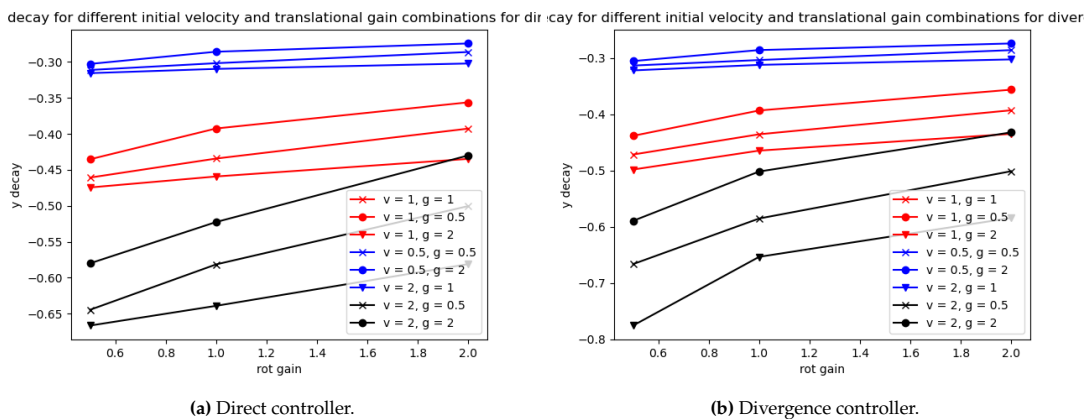
Figure 4.13: Comparison of different initial velocities and gain factors for the two controllers.

4.2. Non ideal hover

Having studied the effects of the different parameters on the behaviour of the controllers, a thorough understanding of the controllers was obtained. Using this understanding it is now possible to make predictions and explain behaviours of the system for more complex situations. The situation that will

Figure 4.14: Realistic sensor decay as function of distance to wall for a focal distance of 1 and decay distance of 3

be studied is one where the assumptions of ideal sensors are loosened to allow for more realistic optical behaviour. Describing first the new non ideal sensor before studying its effects on the behaviour of the controller and the system.

4.2.1. Non ideal sensors

In the original analysis the assumption was made that the optic flow sensor was perfect. The effects of field of view, focal distance and image contrast and change in light intensity do not have an effec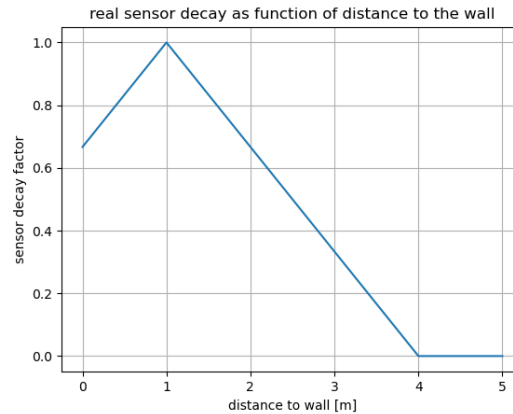t on the optic flow. It was also assumed that from two consecutive images the optic flow can be perfectly obtained. In reality this is not always the case. When it comes to optic flow there are multiple different methods with which optic flow can be obtained. Which can be split into feature based methods and pixel based methods. The first method involves the recognition and tracking of features between the two consecutive images. The optic flow is then obtained by solving Equation 4.1 using the movement of the different features as a set of constraints. Alternatively the assumption is made that between two consecutive images the intensity change of a pixel is minimal. Using this assumption an optic flow vector can be determined for every pixel, by then minimizing a smooth error equation such as suggested by Horn et Schuck [13], one can obtain the optical flow field of an image. Both methods have their advantages for different applications. The method concerning features can be more computer intensive, but might give more accurate results since this method does not solely rely on the assumption of intensity conservation. This method is also not influenced by small changes in focal distance of blurring, since features will still be present although be it in lower contrast. The disadvantage is that field of view and low contrast will hinder feature recognition since features might no longer be visible or warped. Opposed to the feature methods the pixel methods are largely effected by focal distance, image contrast and light intensity. The effect of low contrast, out of focus images and blurring on the optic flow is very similar and is due to the fact that pixel intensity is used to determine optic flow. With low intensity, low contrast or blurred images it is almost impossible to determine the corresponding pixel in the consecutive image with a high measure of accuracy since pixel values are similar.

Within the application of the Atalanta the most likely sensors to be used are sensors based on the pixel method since these are on average smaller in size and requires less computational power. Based on this selection and the discussion of the sensor one way to implement a non ideal sensor is by modeling an additional distance effect, which models the focal distance and affects the intensity of the sensor signal. Other effects such as low contrast images or lighting are harder to model since they are highly environment dependent opposed to focal distance which is sensor dependent. The effect of the modified sensor behaviour can be described by the original sensor behaviour multiplied with an additional function described in Equation 4.2. Here f is the focal distance of the sensor, d the decay distance, the distance from the focal point where the sensor signal reaches zero and lastly x is the distance from the sensor to the wall. Figure 4.14 shows what the decay effect looks like for a focal distance of 1 and a decay distance of 3.

$$\frac{dI}{dx} \cdot V_x + \frac{dI}{dy} \cdot V_y + \frac{dI}{dt} = 0, \tag{4.1}$$

$$h(x) = 1 - \left| \frac{|x| - f}{d} \right|. \tag{4.2}$$

4.2.2. Non ideal hovering behaviour

When non ideal sensors are used, it is expected that for some room sizes and sensor variations the behaviour of the system will drastically change due to the fact that one sensor will produce a significantly stronger signal compered to the other. These cases will most likely occur for short decay distances and large room sizes, given a set focal distance of 1 meter. The exact behavioural change is hard to predict due to the complexity of the sensor and control system, however the expectation is that the decay factor will become lower overall. The effect should be more noticeable for larger rooms, further from the center of the room and for shorter decay distances. Figure 4.15 shows the basic decay results for the different room sizes and sensor decay factors. When comparing these results with the results shown in Figures 4.5 and 4.6 it can be seen that a realistic sensor has a significant effect on the decay behaviour of the system. It can be seen that there some decay factors do not seem to fit the same trend as the other variations of the ideal sensor. In order to effectively analyse this behaviour that does not fit the standard, Figures 4.16 and 4.17 show the time behaviour for the extreme cases. In these time behaviour graphs the horizontal position in the direction of motion is plotted against the vertical position.

(a) X decay direct

(b) Y decay direct

(c) X decay divergence

(d) Y decay divergence
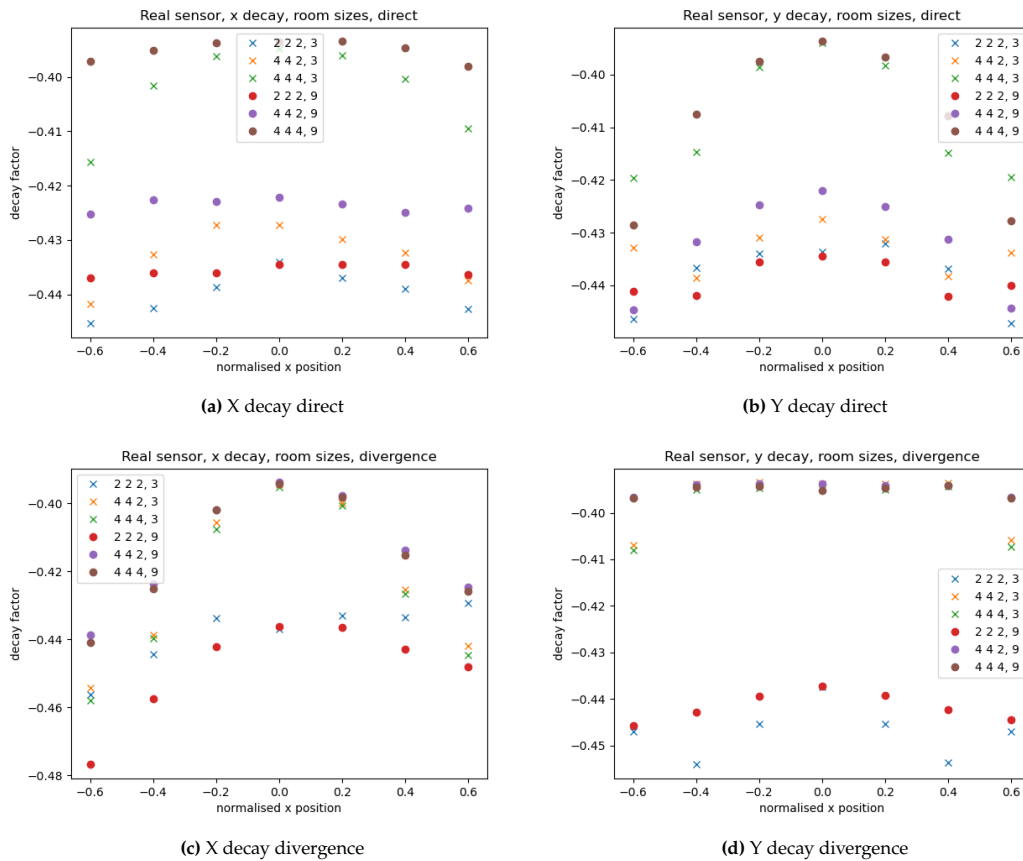
Figure 4.15: Decay behaviour of realistic sensor for different controllers initial velocities and room sizes.

When it comes to the time behaviour for the direct controller at x = 0.0 there is no significant change in the behaviour. However, this changes when moving the initial position towards the wall. When looking at Figures 4.16c and 4.16e it can be seen that specifically the variations with a large room size and small decay distance exhibit different behaviour. This behaviour is unexpected since the effect

occurs when changing the initial position in the direction of motion, where in previous analysis it was shown that this had no effect for the direct controller. The only sensor value that is directly affected by this change in position and the change from ideal to more realistic sensor is the z component of the sensor in the direction of motion. For these exceptional cases, a motion towards the wall results in a very small sensor signal in the negative x direction while resulting in a relatively high sensor signal in the positive x direction as can be seen in Figure 4.18b. This large sensor difference, compared to the center position shown in Figure 4.18a, results in a perceived motion in the z direction significantly stronger than the actual motion of the system. Resulting in the strong asymmetric motion seen in Figures 4.16c and 4.16e. Since this effect is highly dependent on the difference in signal differences it is more prominently present in cases with a short decay distance and a large room size.

For the divergence controller the affected cases are the ones concerning the small rooms. In these specific cases the system seems to respond more strongly when further from the wall compared to closer to the wall as can be best seen in Figure 4.17c. Resulting in a slower response close to the walls compared to the other cases. This is likely due to the fact that for these variations of room size in combination with the sensor decay distance create alternative behaviour. This might originates in the fact that for large rooms the focal distance lays past the wall. Combined with a short decay distance this results in a case where moving away from the wall will result in a stronger signal instead of a weaker one.

(a) X z time behaviour for initial x 0.0

(b) Y z time behaviour for initial x 0.0

(c) X z time behaviour for initial x 0.6

(d) Y z time behaviour for initial x 0.6

(e) X z time behaviour for initial x -0.6

(f) Y z time behaviour for initial x -0.6
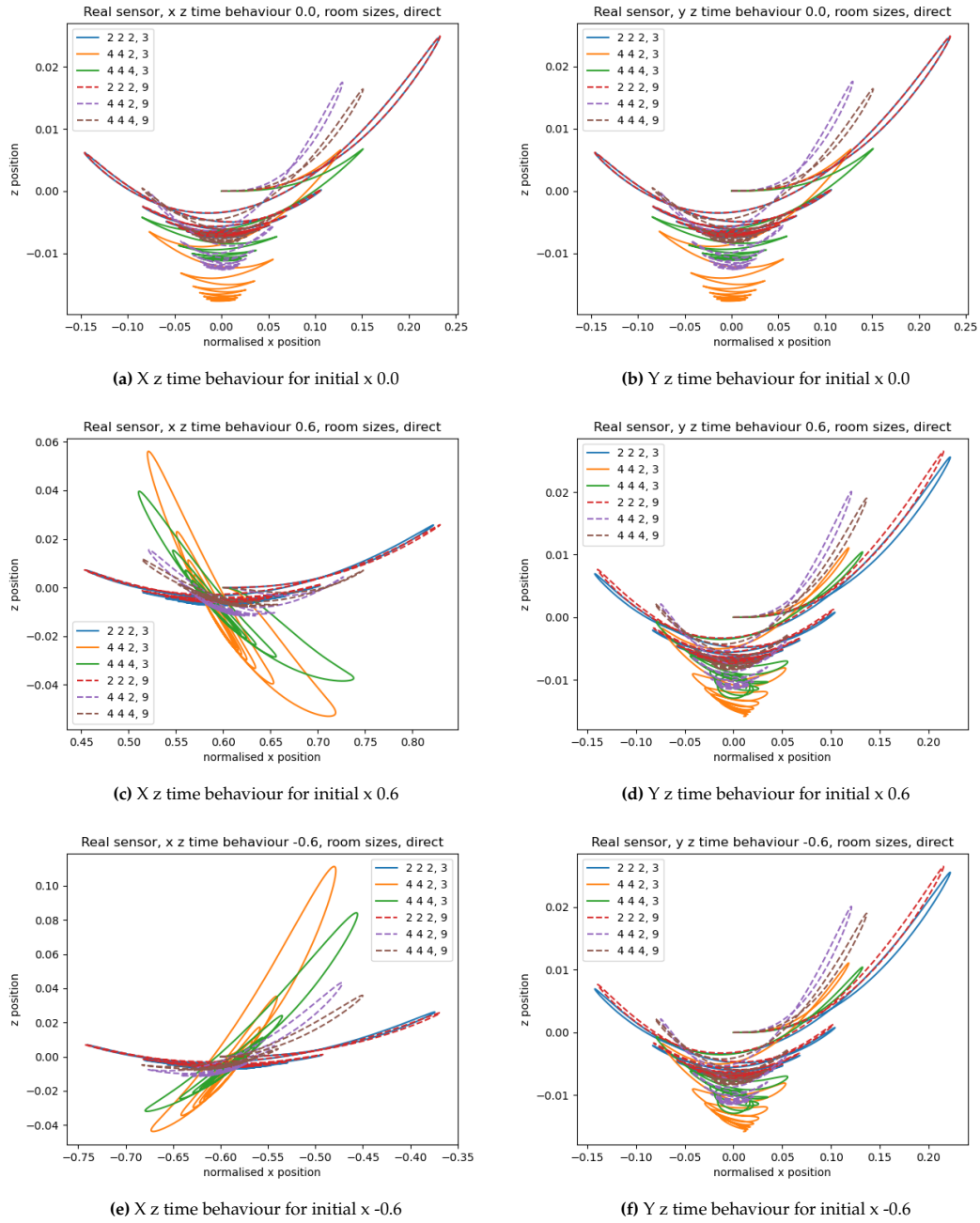
Figure 4.16: Time behaviour of realistic sensor for direct controller with different initial positions, velocities and room sizes

(a) X z time behaviour for initial x 0.0

(b) Y z time behaviour for initial x 0.0

(c) X z time behaviour for initial x 0.6

(d) Y z time behaviour for initial x 0.6

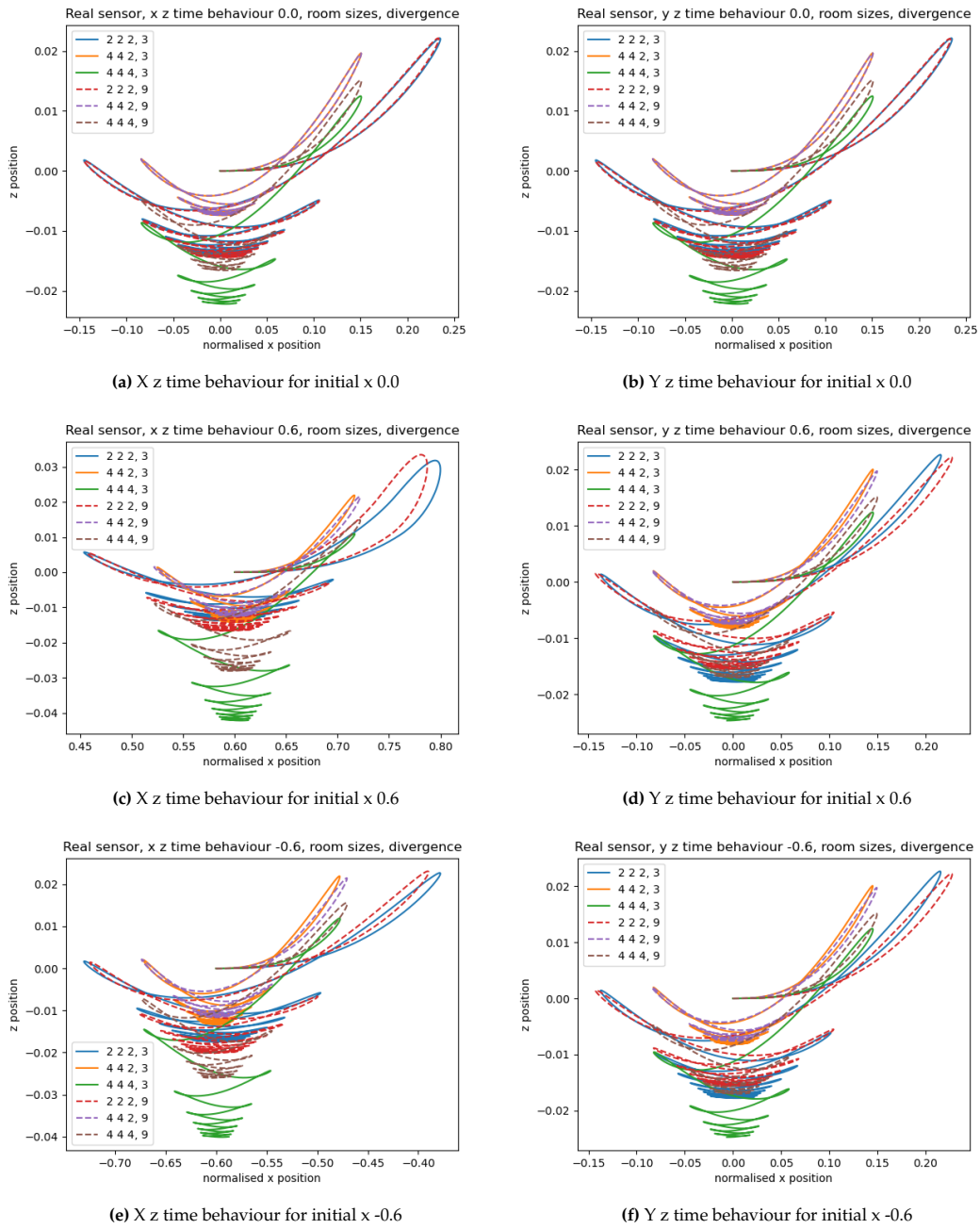(e) X z time behaviour for initial x -0.6

(f) Y z time behaviour for initial x -0.6

Figure 4.17: Time behaviour of realistic sensor for divergence controller with different initial positions, velocities and room sizes

(a) room size of 2x2x2 meter

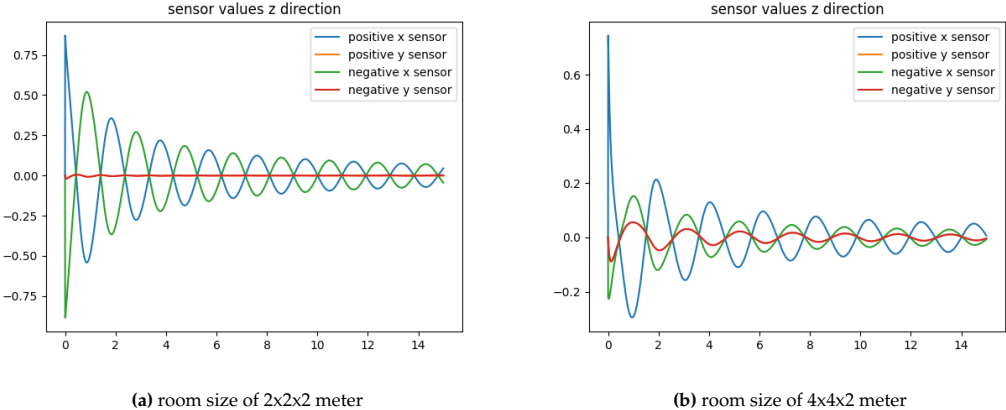**(b)** room size of 4x4x2 meter

Figure 4.18: Time behaviour of z direction optic flow signals for different sensor directions for different room sizes.

5

Discussion

The goal of this master thesis was to develop and analyse a control algorithm for the hovering of the Atalanta FWMAV using optic flow sensors. Due to the fact that the current design of the Atalanta is unable to attain flight, a simulation environment was developed. Within the developed simulation environment the developed control algorithms where tested for a large set of initial condition. Both the direct and divergence controller showed the ability to effecitvely attain a hovering state within a large set of initial condition.

The most important question that now can be answered is which of the two developed controllers is the better one if any. To this question there is no single answer since it was shown that both controllers behave similarly, but show some difference in sensitivity to certain variables. The first important difference between the direct and divergence controllers was observed in the response to initial position, where the divergence controller did not show any significant sensitivity to the initial height. However, the direct controller saw a significant change in the decay where the direction of the height affected whether the change was positive or negative. This difference stemmed from the fact that the direct sensor observes changes perpendicular to the direction of motion, while divergence only observes the effect along the direction of motion. This phenomena is one that plays part in most of the differences between the divergence and direct controllers. This sensitivity to distance was also observed when studying the effect of room size on the behaviour of the controller. It was observed that the divergence controller was only affected by the change of the room size when it corresponded with the direction of motion, while the direct controller was always affected by the change in room size. When it comes to effect of gain on the behaviour of the controllers, they initially respond the same to a small increase or decrease of the gain, but start to deviate for larger gains. For larger gains the divergence has a stronger response compared to the direct controller. This results in the divergence controller becoming unstable at a smaller gain change. This was due to the fact that a gain change resulted in a larger amplitude in the motion, corresponding with a stronger sensor signal and response and therefor better behaviour. Similarly to the ideal sensors, the controllers behave almost the same for the non ideal sensors. This suggests that the effect of the non ideal sensors is not controller dependent, but general. One thing that is significantly different between the two is the time behaviour. The behaviour of the divergence controller is only slightly affected by changes in room size and decay distance, but the behaviour of the direct controller is heavily affected. The slight changes in the behaviour of the divergence controller originates from the fact that when moving away from the wall the sensor signal first becomes stronger before becoming weaker again, opposed to becoming weaker directly resulting in the unexpected behaviour. This however does no affect the stability of the behaviour. The change in the behaviour of the direct controller originate from the z component of the two sensors along the direction of motion. Where the signal decay in these two sensor result in a large difference in the optic flow signal and thereby cause asymmetric behaviour.

In short there are only small differences between the two controllers, where the only significant one is which direction affects the behaviour. The observed differences did not significantly affect the ability of either controller to attain a hovering state, however when a more complex action, such as traversal is required, one of the two might have an advantage. Since the divergence controller is only affected by changes along the direction of motion, it is more suited for navigation and traversal of rooms. The

suitability from the divergence controller stems from the fact that it can observe a wall if it is moving towards allowing for the detection and avoidance of the wall. The direct controller can only detect these walls if there is some motion along the wall. The advantage of the direct controller stems from the fact that it only needs one floor or ceiling in order to detect the motion in the horizontal directions, which allows for the possible control of direction during traversal when no walls are visible.

Based on these analysis a further study should be done which studies the difference between the controllers during traversal. In order to develop a more complete controller capable of fully autonomous or semi controlled flight instead of solely attaining a hovering state. It is also interesting to develop a hybrid controller which uses aspects from both direct and divergence control in order to get the best of both controllers.

References

[1] Markus Achtelik et al. "SFly: Swarm of micro flying robots". In: *2012 IEEE/RSJ International Conference on Intelligent Robots and Systems*. 2012 IEEE/RSJ International Conference on Intelligent Robots and Systems. ISSN: 2153-0866. Oct. 2012, pp. 2649–2650. DOI: `10.1109/IROS.2012.6386281`. URL: `https://ieeexplore.ieee.org/abstract/document/6386281/citations#citations` (visited on 10/13/2023).

[2] C. T. Bolsman. "Flapping wing actuation using resonant compliant mechanisms: An insect-inspired design". In: (2010). Publisher: Ipskamp. URL: `https://repository.tudelft.nl/islandora/object/uuid%3A9c277bea-9b50-4ba4-82c5-09083ffe053a` (visited on 10/26/2023).

[3] Chongjing Cao, Stuart Burgess, and Andrew T. Conn. "Toward a Dielectric Elastomer Resonator Driven Flapping Wing Micro Air Vehicle". In: *Frontiers in robotics and AI* 5 (2018), p. 137. ISSN: 2296-9144. DOI: `10.3389/frobt.2018.00137`.

[4] David Coleman et al. *Design, Development and Flight-Testing of a Robotic Hummingbird*. Vol. 1. Journal Abbreviation: Annual Forum Proceedings - AHS International Publication Title: Annual Forum Proceedings - AHS International. May 6, 2015.

[5] Guido C. H. E. de Croon. "Monocular distance estimation with optical flow maneuvers and efference copies: a stability-based strategy". In: *Bioinspiration & Biomimetics* 11.1 (Jan. 2016). Publisher: IOP Publishing, p. 016004. ISSN: 1748-3190. DOI: `10.1088/1748-3190/11/1/016004`. URL: `https://dx.doi.org/10.1088/1748-3190/11/1/016004` (visited on 09/13/2023).

[6] Shuanghou Deng et al. "Experimental Investigation on the Aerodynamics of a Bio-Inspired Flexible Flapping Wing Micro Air Vehicle". In: *International Journal of Micro Air Vehicles* 6 (June 1, 2014), pp. 105–115. DOI: `10.1260/1756-8293.6.2.105`.

[7] C. P. Ellington. "The novel aerodynamics of insect flight: applications to micro-air vehicles". In: *Journal of Experimental Biology* 202.23 (Dec. 1, 1999), pp. 3439–3448. ISSN: 0022-0949. DOI: `10.1242/jeb.202.23.3439`. URL: `https://doi.org/10.1242/jeb.202.23.3439` (visited on 10/26/2023).

[8] *eMotionButterflies | Festo USA*. URL: `https://www.festo.com/us/en/e/about-festo/research-and-development/bionic-learning-network/highlights-from-2015-to-2017/emotionbutterflies-id_33454/` (visited on 10/27/2023).

[9] J. F. L. Goosen. "Design aspects of a bio-inspired flying sensor node". In: *2012 IEEE SENSORS*. 2012 IEEE SENSORS. ISSN: 1930-0395. Oct. 2012, pp. 1–4. DOI: `10.1109/ICSENS.2012.6411312`.

[10] Lindsey Hines, David Colmenares, and Metin Sitti. "Platform design and tethered flight of a motor-driven flapping-wing system". In: *Proceedings - IEEE International Conference on Robotics and Automation* 2015 (June 29, 2015), pp. 5838–5845. DOI: `10.1109/ICRA.2015.7140016`.

[11] H. W. Ho, G. C. H. E. de Croon, and Q. P. Chu. "Distance and velocity estimation using optical flow from a monocular camera". In: *International Journal of Micro Air Vehicles* 9.3 (2017). ISSN: 1756-8293. DOI: `10.1177/1756829317695566`. URL: `https://repository.tudelft.nl/islandora/object/uuid%3Aa0abc18b-3ee0-4b4e-aac9-c3907a07dd49` (visited on 09/07/2023).

[12] H. W. Ho et al. "Adaptive Gain Control Strategy for Constant Optical Flow Divergence Landing". In: *IEEE Transactions on Robotics* 34.2 (Apr. 2018). Conference Name: IEEE Transactions on Robotics, pp. 508–516. ISSN: 1941-0468. DOI: `10.1109/TRO.2018.2817418`.

[13] Berthold K. P. Horn and Brian G. Schunck. "Determining optical flow". In: *Artificial Intelligence* 17.1 (Aug. 1, 1981), pp. 185–203. ISSN: 0004-3702. DOI: `10.1016/0004-3702(81)90024-2`. URL: `https://www.sciencedirect.com/science/article/pii/0004370281900242` (visited on 09/07/2023).

[14] Noah Jafferis et al. "Untethered flight of an insect-sized flapping-wing microscale aerial vehicle". In: *Nature* 570 (June 1, 2019), pp. 491–495. DOI: `10.1038/s41586-019-1322-0`.

[15] T. Jimbo et al. "Flight control of flapping-wing robot with three paired direct-driven piezoelectric actuators". In: *IFAC-PapersOnLine*. 21st IFAC World Congress 53.2 (Jan. 1, 2020), pp. 9391–9398. ISSN: 2405-8963. DOI: `10.1016/j.ifacol.2020.12.2408`. URL: `https://www.sciencedirect.com/science/article/pii/S2405896320330901` (visited on 10/27/2023).

[16] Matěj Karásek et al. "A tailless aerial robotic flapper reveals that flies use torque coupling in rapid banked turns". In: *Science (New York, N.Y.)* 361.6407 (Sept. 14, 2018), pp. 1089–1094. ISSN: 1095-9203. DOI: `10.1126/science.aat0350`.

[17] Matthew Keennon and Joel Grasmeyer. "Development of Two MAVs and Vision of the Future of MAV Design". In: *AIAA International Air and Space Symposium and Exposition: The Next 100 Years*. International Air and Space Symposium (Evolution of Flight). American Institute of Aeronautics and Astronautics, July 14, 2003. DOI: `10.2514/6.2003-2901`. URL: `https://arc.aiaa.org/doi/10.2514/6.2003-2901` (visited on 10/27/2023).

[18] M. Kharbat et al. *Robust Brightness Description for Computing Optical Flow*. Journal Abbreviation: BMVC 2008 - Proceedings of the British Machine Vision Conference 2008 Publication Title: BMVC 2008 - Proceedings of the British Machine Vision Conference 2008. Jan. 1, 2008. DOI: `10.5244/C.22.46`.

[19] Jayesh Balaji Kottiswaran. "Observations of the quasi-steady aerodynamic model of the Atalanta project for additional velocity conditions". In: (2023). URL: `https://repository.tudelft.nl/islandora/object/uuid%3A7e2448fd-44f1-4711-8901-e3c88a236927` (visited on 09/07/2023).

[20] Kevin Ma and Ronald Fearing. *Efficient Resonant Drive of Flapping-Wing Robots*. Journal Abbreviation: 2009 IEEE/RSJ International Conference on Intelligent Robots and Systems, IROS 2009 Pages: 2860 Publication Title: 2009 IEEE/RSJ International Conference on Intelligent Robots and Systems, IROS 2009. Dec. 11, 2009. 2854 pp. DOI: `10.1109/IROS.2009.5354725`.

[21] Kevin Y. Ma et al. "Controlled Flight of a Biologically Inspired, Insect-Scale Robot". In: *Science* 340.6132 (May 3, 2013). Publisher: American Association for the Advancement of Science, pp. 603–607. DOI: `10.1126/science.1231806`. URL: `https://www.science.org/doi/10.1126/science.1231806` (visited on 10/27/2023).

[22] Mike Menkhorst. "Atalanta Flying Prototype: The Design, Fabrication and Testing of an Uncontrolled Resonant Flapping-Wing Micro Air Vehicle using a Linear Frequency Divider". In: (2023). URL: `https://repository.tudelft.nl/islandora/object/uuid%3A09cfc333-f38a-426a-af93-9586ba23ffd5` (visited on 09/08/2023).

[23] Viet-Quoc Nguyen et al. "Characteristics of an Insect-mimicking Flapping System Actuated by a Unimorph Piezoceramic Actuator". In: *Journal of Intelligent Material Systems and Structures* 19.10 (Oct. 1, 2008). Publisher: SAGE Publications Ltd STM, pp. 1185–1193. ISSN: 1045-389X. DOI: `10.1177/1045389X07084203`. URL: `https://doi.org/10.1177/1045389X07084203` (visited on 10/27/2023).

[24] Hoang Vu Phan et al. "KUBeetle-S: An insect-like, tailless, hover-capable robot that can fly with a low-torque control mechanism". In: *International Journal of Micro Air Vehicles* 11 (Oct. 15, 2019), p. 175682931986137. DOI: `10.1177/1756829319861371`.

[25] D. A. Levinson R. Kane. *Dynamics, Theory and Application*. Dec. 1, 1985. 523 pp.

[26] Leif Ristroph and Stephen Childress. "Stable hovering of a jellyfish-like flying machine". In: *Journal of the Royal Society, Interface / the Royal Society* 11 (Mar. 6, 2014), p. 20130992. DOI: `10.1098/rsif.2013.0992`.

[27] Michelle Rosen et al. *Development of a 3.2g untethered flapping-wing platform for flight energetics and control experiments*. Pages: 3233. May 1, 2016. 3227 pp. DOI: `10.1109/ICRA.2016.7487492`.

[28] A. Roshanbin et al. "COLIBRI: A hovering flapping twin-wing robot". In: *International Journal of Micro Air Vehicles* 9 (Mar. 28, 2017). DOI: `10.1177/1756829317695563`.

[29] Julien R. Serres and Franck Ruffier. "Optic flow-based collision-free strategies: From insects to robots". In: *Arthropod Structure & Development*. From Insects to Robots 46.5 (Sept. 1, 2017), pp. 703–717. ISSN: 1467-8039. DOI: `10.1016/j.asd.2017.06.003`. URL: `https://www.sciencedirect.com/science/article/pii/S146780391730066X` (visited on 09/04/2023).

[30] E. Steltz, S. Avadhanula, and R.S. Fearing. *High lift force with 275 Hz wing beat in MFI*. Pages: 3992. Oct. 1, 2007. 3987 pp. ISBN: 978-1-4244-0912-9. DOI: `10.1109/IROS.2007.4399068`.

[31] Daan van Vrede. "Flight control and collision avoidance for quadcopter and flapping wing MAVs using only optical flow: Theory, Simulation and Experiment". In: (2018). URL: `https://repository.tudelft.nl/islandora/object/uuid%3Ab0394f21-302c-484d-a6dc-031f5860c521` (visited on 09/04/2023).

[32] Robert Wood. "The First Takeoff of a Biologically Inspired At-Scale Robotic Insect". In: *Robotics, IEEE Transactions on* 24 (May 1, 2008), pp. 341–347. DOI: `10.1109/TRO.2008.916997`.

A
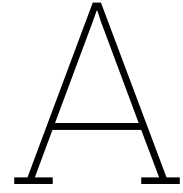
FWMAV project list

In the table below a list of different FWMAV projects over the past two decades can be found. This list has been used as a reference on different achievements and research directions. This table contains only the latest versions of any given project under the assumption that previous work has led to the decision to follow the given line of development. The table shows the different general aspects of the different projects which can be used for classification. Not all projects have attained the same phase in development of their prototype nor have they all shown the same goals for their research and therefore the table can not be used as the sole tool of comparison for the rate of success of the different project. This is furthermore the reason for the incomplete data on some of the listed projects.

Name	Type of sensors	Year of first reference	Type of actuator	Flight obtained?	Type of flight	Wing span	weight
Nano hummingbird [16]	mcu and gyroscope	2005	dc motor	yes	free flight	16 cm	unknown
Atalanta [22]	optic flow	2010	solenoid	no	none	10 cm	Unknown
Microbat [17]	magnetometer, pitot static tube, camera, radio control	2003	Dc motor	yes	free flight	23 cm	Unknown
MFI [30]	No mentioned sensors	1998		no	none	2.6 cm	unknown
LIPCA MAV 2 [23]	no mentioned sensors	2008	Piezo	no	none	12.5 cm	10.28 gram
Microfly [32]	no mentioned sensors	2008	piezo	yes	wired flight	3 cm	0.06 gram
resonant robot[20]	no mentioned sensors	2009	DC motor	no	none		5.9 gram
delfly micro [6]	camera	2012	DC motor	yes	free flight	10 cm	3.07 gram

(Continued)

robobee [21]	external infrared position estimation	2013	Piezo	yes	wired flight	3 cm	0.080 gram
carnegie mav 4 [10]	no mentioned sensors	2015	Piezo	yes	wired flight	14 cm	6.9 gram
jellyfish flyer [26]	no mentioned sensors	2014	DC motor	yes	free flight	10 cm	2.1 gram
hummingbird [4]	no mentioned sensors	2015	DC motor	yes	free flight		62 gram
harvard mav [27]	IMU	2016	DC motor	yes	free flight	16 cm	3.2 gram
Kubeetle-s [24]	gyroscope and magnetometer	2017	DC motor	yes	free flight	15 cm	16.4 gram
colibri [28]	micro mwc multiwii	2017	DC motor	Yes	Free flight	21 cm	22 gram
delfly nimble [16]	Stereo vision	2018	DC motor	yes	free flight	33 cm	28.2 gram
robobee x-wing [14]	No mentioned sensors	2019	piezo	yes	free flight	3.5 cm	0.259 gram
dea mav [3]	No mentioned sensors	2018	dielectric elastomer actuator	no	none	7 cm	10 gram
piezo mav [15]	No mentioned sensors	2020	piezo	yes	wired flight	11.5 cm	1.15 gram
eMotionbutterflies [8]	No mentioned sensors	2015	unkown	yes	free flight	unknown	unkown